Manuscript NCB-D36852

Extracellular matrix mechanical cues regulate lipid metabolism through Lipin-1 and SREBP

Patrizia Romani[1], Irene Brian[1], Giulia Santinon[1], Arianna Pocaterra[1], Matteo Audano[2], Silvia Pedretti[2], Samuel Mathieu[3,4], Mattia Forcato[5], Silvio Bicciato[5], Jean-Baptiste Manneville[3,4], Nico Mitro[2] & Sirio Dupont[1]*

[1]Department of Molecular Medicine (DMM), University of Padua, Padua, Italy
[2]Department of Pharmacological and Biomolecular Sciences (DiSFeB), University of Milan, Milan, Italy
[3]Institut Curie, PSL Research University, CNRS UMR144, Paris, France
[4]Sorbonne Universités, UPMC University Paris 06, CNRS UMR144, Paris, France
[5]Department of Life Sciences, University of Modena and Reggio Emilia, Modena, Italy

*correspondence: sirio.dupont@unipd.it

Extracellular matrix (ECM) mechanical cues have powerful effects on cell proliferation, differentiation and death. Here, starting from an unbiased metabolomics approach, we identified synthesis of neutral lipids as a general response to mechanical signals delivered by cell-matrix adhesions. Extracellular physical cues reverberate on the mechanical properties of the Golgi apparatus and regulate the Lipin-1 phosphatidate phosphatase. Conditions of reduced actomyosin contractility lead to inhibition of Lipin-1, accumulation of SCAP/SREBP to the Golgi apparatus and activation of SREBP transcription factors, in turn driving lipid synthesis and accumulation. This occurs independently of YAP/TAZ, mTOR and AMPK, and in parallel to the feedback control by sterols. Regulation of SREBP can be observed in a stiffened diseased tissue, and contributes to the pro-survival activity of ROCK inhibitors in pluripotent stem cells. We thus identify a general mechanism centered on Lipin-1 and SREBP that links the physical cell microenvironment to a key metabolic pathway.

Introduction

Each tissue has a specific composition of its extracellular matrix (ECM), which is associated to distinctive physical and mechanical properties. These mechanical properties are important for tissue structure, but also control cell function in physiology and disease[1,2]. Cells sense the mechanical properties of the ECM through integrin receptors, and measure them by adjusting the contractility of their F-actin cytoskeleton: contractility is maximal when cells are free to spread on stiff ECM substrata, while it is progressively decreased on a soft ECM or in conditions of limited spreading. This is sufficient to control the switch between proliferation, differentiation and death in very diverse cell types, by regulating intracellular signaling pathways such as YAP/TAZ[3,4] and SRF[5,6]. In support of this model, inhibition of key players that maintain F-actin contractility including the small GTPase RHO, ROCK (RHO kinase), MLCK (myosin light chain kinase) and non-muscle myosin (NMII) induce similar responses to a soft ECM[1]. Yet, what other general aspects of cell biology are regulated by mechanical cues, and through which mechanism(s), remain largely unexplored. This is especially true in the case of metabolism, a fundamental engine that is constantly remodeled to match the energetic and biosynthetic requirements of the cell, whose connections to mechanical cues are only starting to emerge[7,8].

Actomyosin regulates lipid metabolism

To test in an unbiased manner the possibility that actomyosin contractility regulates metabolism we compared by global metabolomics cells in conditions of high contractility (i.e. plated on plastics) with cells in conditions of low contractility, by inhibiting ROCK and MLCK. Analysis of steady-state levels of multiple metabolites indicated clear differences between controls and treated cells (Fig. **1a** and Supplementary Fig. **1a-e**); the most significant and quantitative changes, which were maintained or increased between 6 and 24 hours, were the accumulation of several lipid molecules (Supplementary Fig. **1e** and Ref.[9]).

We validated this initial observation with a targeted lipidomic analysis at 24 hours, which confirmed accumulation of triglycerides, diacylglycerols, lyso-phospholipids and ceramides, while many other lipid species remained overall unchanged (Fig. **1b-d**, Supplementary Fig. **1f-h** and Ref.[9]). This was accompanied by increased free and total fatty acids and cholesterol in cell extracts (Fig. **1e,f**), and by a corresponding accumulation of cholesterol and neutral lipids in fixed cells (by Filipin and Oil-Red-O stains, respectively – Fig. **1g,** Supplementary Fig. **1i-k**). Such accumulation was visible after 6 hours of treatment, and sustained up to 48 hours (Supplementary Fig. **1l**). A similar effect was observed by replacing Y27632 with Fasudil, an alternative ROCK inhibitor, or by using Y27632 or ML7 inhibitors alone (Fig. **1g**). Accumulation of lipids was mainly due to increased synthesis, because it was impaired in cells where rate-limiting enzymes of cholesterol and fatty-acid synthesis were inhibited by Cerivastatin or TOFA (Fig. **1g**). Finally, lipid accumulation was a general response to ECM mechanical cues and actomyosin contractility because expression of the RHO inhibitor C3, treatment of cells with the NMII small-molecule inhibitor Blebbistatin, or seeding cells on a soft vs. stiff fibronectin-coated polyacrylamide hydrogels induced a coherent accumulation of cholesterol and lipid droplets (Fig. **1h-i**). We then extended these findings in multiple cell types including primary, immortalized, and transformed cells, of both epithelial and connective tissue origin, indicating that lipid accumulation is a widespread response to conditions of reduced actomyosin contractility (Fig. **1j,k** and Supplementary Fig. **1m,n**).

ECM mechanical cues regulate a genetic program for lipid synthesis

Thinking of potential mechanisms underlying this metabolic shift, we tested an involvement of the Hippo pathway. YAP/TAZ are inhibited by reduced actomyosin contractility[3,4], but their knockdown did not cause lipid accumulation comparable to ROCK/MLCK inhibition (Supplementary Fig. **2a**). Similarly, stable TAZ-S4A active mutant expression was not sufficient to prevent lipid accumulation upon ROCK/MLCK inhibition (Supplementary Fig. **2b**). LATS1/2 Hippo kinases can be activated by

reduced actomyosin contractility[10], but genetics indicated that LATS2 inhibits lipid metabolism[11], which was incompatible with our results. This suggested the regulation of an alternative pathway that we sought to identify by performing microarray analysis of MCF10ATk1 cells treated with Y27632+ML7, followed by gene list enrichment analysis. As shown in Fig. **2a,b** we found a striking enrichment of signatures related to cholesterol and fatty acid synthesis among the upregulated genes, including many known SREBP1 and SREBP2 (sterol regulatory element binding proteins) targets, pointing to activation of these transcription factors[12,13]. We thus validated activation of SREBP1/2 by a luciferase reporter for SREBP transcriptional activity, by qPCR, and in multiple cell lines (Fig. **2c,d** and Supplementary Fig. **2d-f**). Importantly, we also observed a coherent induction of SREBP target genes in cells cultured on soft hydrogels (Fig. **2e-g**), while YAP/TAZ inhibition had no effects on SREBP activity (Supplementary Fig. **2g,h**). Of note, among the validated SREBP targets *LDLR* (*low density lipoprotein receptor*) expression correlated with increased fatty acid uptake (Supplementary Fig. **2i**), and *ACSS2* (*acyl-CoA synthetase short chain family member 2*) with increased usage of acetate for lipid synthesis[14] (Supplementary Fig. **2j**).

ECM mechanical cues control lipid synthesis through direct regulation of SREBP1/2 activity

SREBP are produced as transmembrane proteins resident in the ER (endoplasmic reticulum) (see model in Supplementary Fig. **3a**): in the presence of sterols and fatty acids, SCAP (SREBP cleavage-activating protein) and Insig (insulin-induced gene) proteins bind SREBP and limit their transport to the Golgi apparatus; in absence of lipids, conformational changes in SCAP and Insig enable the quantitative transport of SCAP and SREBP to the Golgi, where SREBP are processed by the S1P (site-1 protease) and S2P (site-2 protease) Golgi-resident enzymes. This in turn releases the cytoplasmic portion of SREBP that is free to accumulate into the nucleus to regulate gene transcription[12,13].

Prompted by the observation that mechanical cues regulate SREBP activity, we sought to causally link SREBP activity with the effects of mechanical cues. As shown in Fig. **3a-c** and Supplementary Fig. **3b,c** knockdown of SREBP1/2 inhibited expression of lipid enzymes and lipid accumulation in response to Y27632+ML7 and to a soft hydrogel. We then probed endogenous SREBP2 localization and observed an early concentration to the Golgi apparatus (2 hours), closely followed by nuclear accumulation (4-6 hours), upon treatment with ROCK/MLCK inhibitors (Fig. **3d** and Supplementary Fig. **3d-g**). Nuclear accumulation of SREBP2 started to fade at 24 hours and became almost undetectable at 48 hours of treatment (Fig. **3d**), likely due to accumulation of lipids eventually restraining SREBP activation. Moreover, nuclear accumulation was reversible, since

washout of the inhibitors led to the rapid disappearance of nuclear SREBP2 (Fig. **3d**). In keeping with a general effect of mechanical cues, nuclear SREBP2 was observed upon transfection of the C3 RHO inhibitor, treatment with Blebbistatin, and on soft hydrogels (Fig. **3d** and Supplementary Fig. **3f,g**). This was associated with accumulation of cleaved SREBP1 and SREBP2 in nuclear extracts (Fig. **3e** and Supplementary Fig. **3h**). In line with a direct effect, nuclear accumulation of SREBP2 occurred in absence of protein synthesis (Fig. **3f,g** and Supplementary Fig. **3i,j**). Finally, ROCK/MLCK inhibitors could not stimulate further *LDLR-luciferase* in cells engineered to express only a mature form of SREBP2 (Fig. **3h**), indicating regulation of SREBP2 at the level of cleavage and not of nuclear stability.

Inhibition of SREBP activity by pathological tissue stiffness

To find evidence that this regulation also occurs in vivo, we queried gene expression data obtained by comparing patient-matched normal skin with keloid scars[15], a fibroproliferative disorder characterized by increased tissue stiffness and whose expansion is linked to mechanical stress[16,17]. Strikingly, several SREBP target genes were consistently and uniformly downregulated in stiffened keloids across all patients, supporting our model (Fig. **3i**). Of note, this finding nicely parallels the so-far unexplained decrease in lipids and cholesterol-esters observed in keloids[18]. As a control, we also found upregulation of several YAP/TAZ target genes (Fig. **3i**), in line with stiffness-induced YAP/TAZ activity during fibrosis[19,20]. Thus, cytoskeletal tension is a relevant input to regulate SREBP in vitro and in at least one human pathological tissue.

ECM mechanical cues regulate SCAP localization and function

We next probed the subcellular localization of core SREBP regulators. While Insig1 and S1P remained correctly confined to the ER and the Golgi apparatus, respectively (Supplementary Fig. **4a,b**), we observed translocation of SCAP to the Golgi apparatus by plating cells on soft hydrogels and after inhibition of RHO or ROCK/MLCK (Fig. **4a,b** and Supplementary Fig. **4c**). This was instrumental for the regulation of SREBP by mechanical cues, because both SCAP knockdown and treatment of cells with 25-hydroxycholesterol, a dominant inhibitor of SCAP transport[21], decreased SREBP activation (Fig. **4c,e** and Supplementary Fig. **4d**). In line, treating cells with the S1P inhibitor PF429242 also prevented activation of SREBP (Fig. **4d,e**). This indicates that actomyosin contractility prevents accumulation of SCAP/SREBP to the Golgi apparatus and the exposure of SREBP to Golgi proteases.

Lipid synthesis contributes to the beneficial effects of ROCK inhibitors in hPSC

To expand the functional implications of these findings we used human Pluripotent Stem Cells (hPSC). These cells require treatment with the Y27632 ROCK inhibitor to survive single-cell dissociation, while they thrive without inhibitor once they have attached to the substrate[22,23]. We thus tested the idea that Y27632 might promote survival of hPSC by enhancing lipid synthesis. We first confirmed that Y27632 induces lipid accumulation also in these cells (Supplementary Fig. **4e**). We then challenged Y27632-induced survival of hPSC seeded as single cells by using very low doses of lipid synthesis inhibitors (Cerivastatin and TOFA), and found that hPSC did not survive (Fig. **4f**, single cells); the same dose of inhibitors was instead inconsequential for cell survival of already-established hPSC colonies, when Y27632 is not required (Fig. **4f**, colonies). In line, both treatment of cells with 25-hydroxycholesterol and transfection of SREBP1/2 siRNAs impaired Y27632-induced single-cell survival (Fig. **4g,h**). These results suggest that isolated hPSC are highly dependent on lipid synthesis, and that ROCK inhibition promotes their survival, at least in part, by sustaining SREBP activity.

Uncoupling actomyosin contractility from intracellular cholesterol trafficking

One possibility to explain our findings is that reduced actomyosin contractility leads to reduced levels of sterols at the ER because of decreased transport of extracellular cholesterol from the endosome/lysosome to the ER by the NPC1 transporter[12,13]. We excluded this scenario based on the following observations: (i) cholesterol accumulation in response to Y27632+ML7 was decreased in cells with inhibited synthesis or with SREBP1/2 knockdown (see above), indicating it is a secondary effect; (ii) cholesterol accumulation occurred after SREBP activation, and with a delayed kinetics compared to inhibition of the NPC1 transporter with U18666A (Supplementary Fig. **5a**); (iii) while U18666A induced accumulation of cholesterol in LAMP2-encircled lysosomal structures, as expected, only few Y27632+ML7-induced cholesterol dots were positive for LAMP2 (Supplementary Fig. **5b**); (iv) treatment with Y27632+ML7, at difference with U18666A or with serum (and, thus, LDL-cholesterol) deprivation, did not cause concentration of the ER cholesterol-sensing protein OSBP to the Golgi apparatus at early time-points[24,25] (Supplementary Fig. **5c**).

Linking actomyosin contractility to the Lipin-1/ARF1 SREBP-regulatory axis

Looking for alternative mechanisms, we reasoned that among the known SREBP-regulatory inputs, two act independently of sterol levels: ARF1 and Lipin-1. The ARF1 (ADP ribosylation factor 1) small G protein regulates Golgi dynamics[26,27], and inhibits SREBP[28-30]. The precise mechanism remained

incompletely understood, because Walker and colleagues showed that ARF1 prevents S1P from shuttling to the ER, while Nakayama and colleagues showed that the ARF1 effector COPI prevents accumulation of SCAP/SREBP to the Golgi. Lipin-1 is a phosphatase that converts phosphatidates into diacylglycerols at cytoplasmic membranes[31], and also an inhibitor of SREBP activity[29,32]. Interestingly, ARF1 recruitment to the Golgi apparatus and formation of COPI-coated vesicles requires diacylglycerols[33-36], such that inhibition of Lipin-1 activity can cause ARF1 dissociation from Golgi membranes and ARF1 inhibition[29,35]. This suggested us that reduced actomyosin contractility might induce SREBP activity by inhibiting Lipin-1/ARF1 (see model in Supplementary Fig. **5d**).

We first verified that inhibition of Lipin-1, ARF1 or COPI induce SREBP activation, SCAP accumulation at the Golgi apparatus and lipid accumulation in our systems (Fig. **5a-f** and Supplementary Fig. **5e**). We then indirectly gauged Lipin-1 activity by monitoring its association with microsomes[37,38] or by monitoring Golgi membrane diacylglycerol (DG) content with the DG-binding domain of PKD1 (GFP-PKD-KD)[35,39,40], and found that inhibition of ROCK/MLCK rapidly caused Lipin-1 dissociation from microsomes (Fig. **5g**) and decreased GFP-PKD-KD co-localization with the Golgi apparatus (Fig. **5h**). ROCK/MLCK inhibition also decreased ARF1 activity (Fig. **5i**) and ARF1 recruitment to the Golgi apparatus (Fig. **5j**). Moreover, both Lipin-1 and ROCK/MLCK inhibition induce similar remodeling of Golgi morphology at late time-points (Supplementary Fig. **5f,g**), a phenotype previously observed in cells depleted of GBF1/ARF1[28]. We did not observe a general redistribution of a fluorescent KDEL reporter (Supplementary Fig. **5h**), indicating overall intact transports between ER and Golgi. Collectively, our data indicate that mechanical cues control Lipin-1 activity, causing altered ARF1-dependent trafficking of SCAP/SREBP between the Golgi and the ER.

Actomyosin contractility controls SREBP through Lipin-1, but independently from AMPK/mTOR

We then explored how Lipin-1 is regulated. Lipin-1 activity and association to cytoplasmic membranes can be inhibited by phosphorylation[32,37,38]. We checked Lipin-1 overall phosphorylation levels, but we did not observe major changes of the Lipin-1 migratory pattern (Fig. **6a**). We also monitored Lipin-1 subcellular localization by immunofluorescence, and found that reduced contractility partially shifted FLAG-Lipin-1 towards the nucleus (Fig. **6b,c**). Nuclear Lipin-1 has been associated with inactivation of SREBP[32]; since we observed a partial nuclear accumulation of Lipin-1 in conditions of active SREBP, we then wondered what pool of Lipin-1 was relevant in our cells. For this we compared wild-type Lipin-1 (WT) with a nuclear phospho-mutant (17S/A) and with Lipin-1 isoforms that we designed

to constitutively associate with ER/Golgi membranes (MB-Lipin-1 and MB*-Lipin-1 - see Fig. **6c**), and used these to challenge the effects of reduced contractility. While the WT and 17S/A mutant were inactive, expression of membrane-associated Lipin-1 counteracted SREBP activity (Fig. **6d,e**) and lipid accumulation (Fig. **6f**). Also the SUMOylation[41] and acetylation[42] Lipin-1 mutants were inactive in the same assay (Supplementary Fig. **6a**). Collectively, these results indicate that reduced contractility inhibits the affinity of Lipin-1 for ER/Golgi membranes, leading to nuclear localization of Lipin-1 as secondary effect. This occurs independently from mTOR, a known Lipin-1 regulatory input (Supplementary Fig. **6b,c**), and also from AMPK, a main metabolic regulator (Supplementary Fig. **6d,e**).

The Golgi apparatus responds to extracellular and intracellular forces

We finally sought to obtain some insight into how extracellular mechanical cues influence signaling at the Golgi apparatus. Transmission of forces from the ECM entail activation of signaling molecules at focal adhesions[1] but also occur in a direct fashion, for example by stretching the plasma membrane, or owing to anchoring of stress fibers to the nuclear lamina[43,44]. Whether the Golgi apparatus might respond in a similar fashion has not been explored, but Golgi cisternae are embedded in a complex cytoskeletal network[45,46], and the Golgi microenvironment is endowed of an intrinsic mechanical rigidity which depends on ROCK/MLCK[47]. To measure the response of Golgi rigidity to external physical cues we plated cells on small fibronectin-coated micropatterns, to which cells respond by decreasing actomyosin contractility[48], and by accumulating SCAP to the Golgi apparatus (Fig. **7a**).We then measured Golgi rheology by pushing on the Golgi apparatus a cytoplasmic bead immobilized in a laser optical trap (see methods and Supplementary Fig. **7a**). Analysis of the averaged relaxation curves (Fig. **7b** and Supplementary Fig. **7b**) indicated a lower rigidity of the Golgi apparatus in micropatterned cells, apparent from reduction of the bead step amplitude, the rigidity index, and the frequency of bead ejection (Fig. **7c**). As a control, moving the bead away from the Golgi showed that the overall cytoplasmic stiffness is not altered (Supplementary Fig. **7c**). This experiment indicates that Golgi stiffness is coupled, directly or indirectly, to the mechanical properties of the ECM. Strikingly, with this set-up we also observed that direct application of force to the Golgi apparatus was sufficient to induce recruitment of the GFP-PKD-KD reporter (Fig. **7d,e**), in line with higher Lipin-1 activity in cells developing higher contractile forces (see above).

Discussion

Seminal work demonstrating that cells sense ECM mechanical cues set the array of bona-fide mechanoregulated phenotypes in vitro. Yet, what other general cell phenotypes are regulated by mechanical cues remains largely unexplored. Here we focused on cell metabolism and identified neutral lipid and cholesterol synthesis as a general response to reduced actomyosin contractility and to a soft ECM microenvironment. We propose that decreased extracellular forces reverberate on Golgi rheology and inactivate Lipin-1, causing alteration of diacylglycerol at the Golgi apparatus, reduced recruitment of ARF1, and ultimately leading to activation of SREBP1/2 transcription factors. As such, our data provide a missing upstream input for the Lipin-1 and ARF1 SREBP-regulatory axis, whose players were previously identified in *C. elegans*[29], and validates the idea that continuous shuttling of SCAP/SREBP from the Golgi to the ER is a significant mechanism limiting their activation[30]. These findings led us to revisit the requirement of isolated human pluripotent stem cells for ROCK inhibition, that we found linked to the ability to sustain SREBP activity and lipid synthesis. We speculate this might underlie the beneficial effect of ROCK inhibition observed for isolation of other primary stem-cell populations[49-51]. These findings also indicate that physiological or pathological conditions leading to altered tissue stiffness may impact SREBP activity and lipid metabolism; strikingly, we could obtain a proof-of-principle for this in human keloid scars, providing a plausible explanation for reduced triglycerides and cholesteryl-esters[18]. Thus, we here identify an unexpected and widespread mechanoresponsive phenotype, and its main underlying mechanism. Our findings raise interesting questions on how Lipin-1 is regulated in this context; we speculate that Lipin-1 macromolecular complexes observed on supported lipid bilayers in vitro[52] are endowed of curvature-sensing ability, which might link Lipin-1 activity to the rheology of Golgi membranes and the cytoskeleton. In future, it will be interesting to test whether ECM mechanical cues affect other functions of the Golgi, of Lipin-1 signaling and of ARF1, and how these impact the response of normal and diseased tissues to mechanical cues.

References

1. Iskratsch, T., Wolfenson, H. & Sheetz, M. P. Appreciating force and shape—the rise of mechanotransduction in cell biology. *Nat. Rev. Mol. Cell Biol.* **15,** 825–833 (2014).
2. LeGoff, L. & Lecuit, T. Mechanical Forces and Growth in Animal Tissues. *Cold Spring Harbor Perspectives in Biology* **8,** a019232 (2015).
3. Dupont, S. *et al.* Role of YAP/TAZ in mechanotransduction. *Nature* **474,** 179–183 (2011).
4. Dupont, S. Role of YAP/TAZ in cell-matrix adhesion-mediated signalling and mechanotransduction. *Exp. Cell Res.* **343,** 42–53 (2016).
5. Miralles, F., Posern, G., Zaromytidou, A.-I. & Treisman, R. Actin dynamics control SRF activity by regulation of its coactivator MAL. *Cell* **113,** 329–342 (2003).

6. Janmey, P. A., Wells, R. G., Assoian, R. K. & McCulloch, C. A. From tissue mechanics to transcription factors. *Differentiation* **86,** 112–120 (2013).
7. Coloff, J. L. *et al.* Differential Glutamate Metabolism in Proliferating and Quiescent Mammary Epithelial Cells. *Cell Metabolism* **23,** 867–880 (2016).
8. Bays, J. L., Campbell, H. K., Heidema, C., Sebbagh, M. & DeMali, K. A. Linking E-cadherin mechanotransduction to cell metabolism through force-mediated activation of AMPK. *Nat. Cell Biol.* **19,** 724–731 (2017).
9. Romani, P. *et al.* Metabolomics and Lipidomics analyses of MCF10ATk1 cells treated with ROCK/MLCK inhibitors. *Figshare database* (2018). doi:10.6084/m9.figshare.7338764
10. Zhao, B. *et al.* Cell detachment activates the Hippo pathway via cytoskeleton reorganization to induce anoikis. *Genes Dev.* **26,** 54–68 (2012).
11. Aylon, Y. *et al.* The LATS2 tumor suppressor inhibits SREBP and suppresses hepatic cholesterol accumulation. *Genes Dev.* (2016). doi:10.1101/gad.274167.115
12. Shimano, H. & Sato, R. SREBP-regulated lipid metabolism: convergent physiology - divergent pathophysiology. *Nat Rev Endocrinol* (2017). doi:10.1038/nrendo.2017.91
13. Brown, M. S., Radhakrishnan, A. & Goldstein, J. L. Retrospective on Cholesterol Homeostasis: The Central Role of Scap. *Annu. Rev. Biochem.* **87,** annurev–biochem–062917–011852 (2017).
14. Comerford, S. A. *et al.* Acetate Dependence of Tumors. *Cell* **159,** 1591–1602 (2014).
15. Hsu, C.-K. *et al.* Caveolin-1 Controls Hyperresponsiveness to Mechanical Stimuli and Fibrogenesis-Associated RUNX2 Activation in Keloid Fibroblasts. *J. Invest. Dermatol.* (2017). doi:10.1016/j.jid.2017.05.041
16. Ogawa, R. Mechanobiology of scarring. *Wound Repair Regen* **19 Suppl 1,** s2–9 (2011).
17. Aya, R. *et al.* The Shear Wave Velocity on Elastography Correlates with the Clinical Symptoms and Histopathological Features of Keloids. *Plastic and Reconstructive Surgery Global Open* **3,** e464 (2015).
18. Tachi, M. & Iwamori, M. Mass spectrometric characterization of cholesterol esters and wax esters in epidermis of fetal, adult and keloidal human skin. *Experimental Dermatology* **17,** 318–323 (2008).
19. Calvo, F. *et al.* Mechanotransduction and YAP-dependent matrix remodelling is required for the generation and maintenance of cancer-associated fibroblasts. *Nat. Cell Biol.* **15,** 637–646 (2013).
20. Liu, F. *et al.* Mechanosignaling through YAP and TAZ drives fibroblast activation and fibrosis. *Am. J. Physiol. Lung Cell Mol. Physiol.* **308,** L344–57 (2015).
21. Sun, L.-P., Seemann, J., Goldstein, J. L. & Brown, M. S. Sterol-regulated transport of SREBPs from endoplasmic reticulum to Golgi: Insig renders sorting signal in Scap inaccessible to COPII proteins. *Proc. Natl. Acad. Sci. U.S.A.* **104,** 6519–6526 (2007).
22. Watanabe, K. *et al.* A ROCK inhibitor permits survival of dissociated human embryonic stem cells. *Nat Biotechnol* **25,** 681–686 (2007).
23. Ohgushi, M. *et al.* Molecular pathway and cell state responsible for dissociation-induced apoptosis in human pluripotent stem cells. *Cell Stem Cell* **7,** 225–239 (2010).
24. Storey, M. K., Byers, D. M., Cook, H. W. & Ridgway, N. D. Cholesterol regulates oxysterol binding protein (OSBP) phosphorylation and Golgi localization in Chinese hamster ovary cells: correlation with stimulation of sphingomyelin synthesis by 25-hydroxycholesterol. *Biochem. J.* **336 (Pt 1),** 247–256 (1998).
25. Mohammadi, A. *et al.* Golgi localization and phosphorylation of oxysterol binding protein in Niemann-Pick C and U18666A-treated cells. *J. Lipid Res.* **42,** 1062–1071 (2001).
26. De Matteis, M. A. & Godi, A. Protein-lipid interactions in membrane trafficking at the Golgi complex. *Biochim. Biophys. Acta* **1666,** 264–274 (2004).
27. D'Souza-Schorey, C. & Chavrier, P. ARF proteins: roles in membrane traffic and beyond. *Nat.*

Rev. Mol. Cell Biol. **7,** 347–358 (2006).
28. Walker, A. K. *et al.* A conserved SREBP-1/phosphatidylcholine feedback circuit regulates lipogenesis in metazoans. *Cell* **147,** 840–852 (2011).
29. Smulan, L. J. *et al.* Cholesterol-Independent SREBP-1 Maturation Is Linked to ARF1 Inactivation. *CellReports* **16,** 9–18 (2016).
30. Takashima, K. *et al.* COPI-mediated retrieval of SCAP is crucial for regulating lipogenesis under basal and sterol-deficient conditions. *J. Cell. Sci.* **128,** 2805–2815 (2015).
31. Zhang, P. & Reue, K. Lipin proteins and glycerolipid metabolism: Roles at the ER membrane and beyond. *Biochim. Biophys. Acta* **1859,** 1583–1595 (2017).
32. Peterson, T. R. *et al.* mTOR Complex 1 Regulates Lipin 1 Localization to Control the SREBP Pathway. *Cell* **146,** 408–420 (2011).
33. Fernández-Ulibarri, I. *et al.* Diacylglycerol is required for the formation of COPI vesicles in the Golgi-to-ER transport pathway. *Mol. Biol. Cell* **18,** 3250–3263 (2007).
34. Asp, L. *et al.* Early stages of Golgi vesicle and tubule formation require diacylglycerol. *Mol. Biol. Cell* **20,** 780–790 (2009).
35. Baron, C. L. & Malhotra, V. Role of diacylglycerol in PKD recruitment to the TGN and protein transport to the plasma membrane. *Science (New York, N.Y.)* **295,** 325–328 (2002).
36. Antonny, B., Huber, I., Paris, S., Chabre, M. & Cassel, D. Activation of ADP-ribosylation factor 1 GTPase-activating protein by phosphatidylcholine-derived diacylglycerols. *Journal of Biological Chemistry* **272,** 30848–30851 (1997).
37. Harris, T. E. *et al.* Insulin controls subcellular localization and multisite phosphorylation of the phosphatidic acid phosphatase, lipin 1. *Journal of Biological Chemistry* **282,** 277–286 (2007).
38. Péterfy, M., Harris, T. E., Fujita, N. & Reue, K. Insulin-stimulated interaction with 14-3-3 promotes cytoplasmic localization of lipin-1 in adipocytes. *J. Biol. Chem.* **285,** 3857–3864 (2010).
39. Hausser, A. *et al.* Protein kinase D regulates vesicular transport by phosphorylating and activating phosphatidylinositol-4 kinase IIIbeta at the Golgi complex. *Nat. Cell Biol.* **7,** 880–886 (2005).
40. Villani, M. *et al.* Sphingomyelin synthases regulate production of diacylglycerol at the Golgi. *Biochem. J.* **414,** 31–41 (2008).
41. Liu, G.-H. & Gerace, L. Sumoylation regulates nuclear localization of lipin-1alpha in neuronal cells. *PLoS ONE* **4,** e7031 (2009).
42. Li, T. Y. *et al.* Tip60-mediated lipin 1 acetylation and ER translocation determine triacylglycerol synthesis rate. *Nat Comms* **9,** 1916 (2018).
43. Isermann, P. & Lammerding, J. Nuclear Mechanics and Mechanotransduction in Health and Disease. *Current Biology* **23,** R1113–R1121 (2013).
44. Coste, B. *et al.* Piezo1 and Piezo2 are essential components of distinct mechanically activated cation channels. *Science (New York, N.Y.)* **330,** 55–60 (2010).
45. Egea, G., Lázaro-Diéguez, F. & Vilella, M. Actin dynamics at the Golgi complex in mammalian cells. *Curr. Opin. Cell Biol.* **18,** 168–178 (2006).
46. Gurel, P. S., Hatch, A. L. & Higgs, H. N. Connecting the Cytoskeleton to the Endoplasmic Reticulum and Golgi. *Current Biology* **24,** R660–R672 (2014).
47. Guet, D. *et al.* Mechanical role of actin dynamics in the rheology of the Golgi complex and in Golgi-associated trafficking events. *Current biology : CB* **24,** 1700–1711 (2014).
48. Fu, J. *et al.* Mechanical regulation of cell function with geometrically modulated elastomeric substrates. *Nat. Methods* **7,** 733–736 (2010).
49. Sato, T. & Clevers, H. Growing self-organizing mini-guts from a single intestinal stem cell: mechanism and applications. *Science (New York, N.Y.)* **340,** 1190–1194 (2013).

50. McFarlane, M. R. *et al.* Scap is required for sterol synthesis and crypt growth in intestinal mucosa. *J. Lipid Res.* **56,** 1560–1571 (2015).
51. Katsuda, T. *et al.* Conversion of Terminally Committed Hepatocytes to Culturable Bipotent Progenitor Cells with Regenerative Capacity. *Cell Stem Cell* **20,** 41–55 (2017).
52. Creutz, C. E., Eaton, J. M. & Harris, T. E. Assembly of high molecular weight complexes of lipin on a supported lipid bilayer observed by atomic force microscopy. *Biochemistry* **52,** 5092–5102 (2013).
53. Watson, R. T. & Pessin, J. E. Transmembrane domain length determines intracellular membrane compartment localization of syntaxins 3, 4, and 5. *Am. J. Physiol., Cell Physiol.* **281,** C215–23 (2001).
54. Misumi, Y., Sohda, M., Tashiro, A., Sato, H. & Ikehara, Y. An essential cytoplasmic domain for the Golgi localization of coiled-coil proteins with a COOH-terminal membrane anchor. *Journal of Biological Chemistry* **276,** 6867–6873 (2001).
55. Enzo, E. *et al.* Aerobic glycolysis tunes YAP/TAZ transcriptional activity. *EMBO J.* **34,** 1349–1370 (2015).
56. Aragona, M. *et al.* A mechanical checkpoint controls multicellular growth through YAP/TAZ regulation by actin-processing factors. *Cell* **154,** 1047–1059 (2013).
57. Santinon, G. *et al.* dNTP metabolism links mechanical cues and YAP/TAZ to cell growth and oncogene-induced senescence. *EMBO J.* **37,** e97780 (2018).
58. Irizarry, R. A. *et al.* Exploration, normalization, and summaries of high density oligonucleotide array probe level data. *Biostatistics* **4,** 249–264 (2003).
59. Tusher, V. G., Tibshirani, R. & Chu, G. Significance analysis of microarrays applied to the ionizing radiation response. *Proc. Natl. Acad. Sci. U.S.A.* **98,** 5116–5121 (2001).
60. Kuleshov, M. V. *et al.* Enrichr: a comprehensive gene set enrichment analysis web server 2016 update. *Nucleic Acids Res.* **44,** W90–7 (2016).
61. Horton, J. D. *et al.* Combined analysis of oligonucleotide microarray data from transgenic and knockout mice identifies direct SREBP target genes. *Proc. Natl. Acad. Sci. U.S.A.* **100,** 12027–12032 (2003).
62. Porstmann, T. *et al.* PKB/Akt induces transcription of enzymes involved in cholesterol and fatty acid biosynthesis via activation of SREBP. *Oncogene* **24,** 6465–6481 (2005).
63. Mandal, K., Asnacios, A., Goud, B. & Manneville, J.-B. Mapping intracellular mechanics on micropatterned substrates. *Proceedings of the National Academy of Sciences* **113,** E7159–E7168 (2016).

Acknowledgements

We are grateful to Y. Chen, K. Mori, G. DelSal, B. Viollet and H. Louvel, E. Greotti, A. DeMatteis and R. Venditti, A. Hausser, R. Rizzuto and D. Vecellio Reane, L. Scorrano and L. Pernas, C. Cheng, E. Melloni, M. Pende and R. Talha, R. Ogawa, J. Goldstein P. Espenshade and W. Shao for advice and materials. We are indebted to S. Giulitti for generous help with hydrogels, to M. Pellegrini and I. Zorzan for help with hPSC cultures, to G. Martello and M. Montagner for thoughtful discussion. This work was supported by AIRC IG-15307, WCR 15-1192, CARIPARO Eccellenza 2017 and University of Padua BIRD grants to SD, AIRC 'Hard ROCK Café Fellowship to GS, UPMC 'Interface pour le Vivant' doctoral program to SM, AIRC Special Program Molecular Clinical Oncology '5 per mille' 10016 to SB.

Author contributions

PR and IB performed experiments and analyzed data with help from GS and AP; MA and SP and NM performed metabolic measurements and advised on the interpretation of metabolic data; SM and JBM performed Golgi micromanipulations; MF and SB performed bioinformatics analyses; SD and PR planned experiments; SD coordinated and supervised the project, and wrote the paper.

Competing Interests

The authors declare no competing or financial interests.

Figure legends

Figure 1. Actomyosin contractility and ECM mechanical cues regulate lipid synthesis.
a, Principal component analysis of metabolites altered by global metabolomics in MCF10ATk1 human mammary epithelial cells treated for 6 or 24 hours with 20μM Y27632 ROCK inhibitor and 20μM ML7 MLCK inhibitor to inhibit actomyosin contractility (hereafter YM, n=6 biologically independent samples), as compared to vehicle (DMSO, n=4 biologically independent samples). **b,** Volcano plot of lipid molecules altered in MCF10ATk1 cells treated for 24 hours with YM, as measured by targeted lipidomics. n=5 biologically independent samples per condition. TG, triacylglycerols; DG, diacylglycerols; LysoPC, lyso-phosphatidylcholines; Cer, ceramides. **c,d,** TG (**c**) and DG (**d**) levels in MCF10ATk1 cells treated with YM for 24 hours, as measured by mass spectrometry. Only the five most abundant species are shown. **e,f,** Fatty acids (**e,** n=5 biologically independent samples per condition) and cholesterol (**f,** n=9 biologically independent samples per condition) in MCF10ATk1 cells treated with YM, as assayed by standard colorimetric assays. **g,** Filipin staining for cholesterol and Oil-Red-O staining (ORO) for neutral lipids in MCF10ATk1 cells treated with YM or FM (Fasudil+ML7). Inhibition of cholesterol and fatty acid synthesis with 10μM Cerivastatin (Ceri) or with 15μM TOFA prevents accumulation. Here and through all figures, image acquisition settings were the same between controls and experimental samples. Scale bar 5μm. **h,** Accumulation of cholesterol and neutral lipids in MCF10ATk1 cells upon inhibition of RHO (C3 transferase transfection), non-muscle myosin II (20μM Blebbistatin) or by plating cells on soft (E≈0.5kPa) fibronectin-coated polyacrylamide hydrogels, compared to stiff (E≈15kPa) hydrogels. Scale bar 5μm. **i,** Transmission electron microscope pictures of MCF10ATk1 cells plated on stiff or soft hydrogel, with apparent lipid droplets (LD) and part of the nucleus (N). Scale bar 1μm. **j,k,** non-transformed human RPE1 (**j**) and primary mouse 3T3L1 (**k**) cells plated on stiff or soft hydrogels. Scale bar 5μm. The images in panels **g-k** are representative of at least two independent experiments with similar results; quantifications and n are provided in Supplementary Table 2. Data are mean and single points; unpaired two-tailed Student's t-tests.

Figure 2. ECM mechanical cues regulate SREBP1/2 target genes.
a, Gene list enrichment analysis on probes significantly upregulated (mean fold>1.3 $P<0.05$) in microarrays of MCF10ATk1 cells treated with DMSO or Y27632+ML7 (YM) for 6 hours. The graphs display the 10 most significantly overrepresented gene sets for each of the indicated databases, analyzed with Enrichr and ranked according to combined score (x axis). Gene sets related to cholesterol, lipids and SREBP are highlighted in orange. **b,** Heatmap of SREBP target genes in microarrays of MCF10ATk1 cells treated as in **a**. Each column is an independent biological sample (n=3 for each condition); each line corresponds to a single gene probe indicated on the right. Blue and yellow extremes correspond to raw Z-scores of -2 and +2, respectively. **c,** *LDLR-luciferase* reporter assay for SREBP activity in MDA231 cells treated with YM or Fasudil+ML7 (FM). Mean expression in controls was set to 1, and other samples are relative to this (n≥6 independent biological samples per condition; unpaired Mann-Whitney tests). **d,** qPCR for established SREBP targets in RPE1 cells treated for 6 or 24 hours with DMSO, YM or FM (n≥4 independent biological samples per condition; multiple unpaired two-tailed Student's t-tests). **e-g,** qPCR for established SREBP targets in MCF10ATk1 (**e**), RPE1 (**f**) or 3T3L1 (**g**) cells plated on stiff (E≈15kPa) or soft (E≈0.5kPa) ECM-coated hydrogels for 24 hours (n≥4 independent biological samples per condition; multiple unpaired two-tailed Student's t-tests). In **d-g** data are relative to *GAPDH* levels; mean expression in controls (DMSO or stiff) were set to 1, and all other samples are relative to this. Data are mean and single points.

Figure 3. ECM mechanical cues regulate lipid synthesis by controlling SREBP1/2 activation.
a, qPCR analysis in MCF10ATk1 cells 48 hours after transfection with control siRNA (siCo.) or four independent mixes of siRNAs targeting *SREBF1* and *SREBF2* mRNAs (siSREBP A to D). **b,** qPCR analysis of established SREBP1/2 targets in MCF10ATk1 transfected as in **a** and treated with DMSO or YM for 24 hours. In **a** and **b** mRNA expression data are relative to *GAPDH* levels; mean expression levels in controls was set to 1, and all other samples are expressed relative to this (n≥4 independent biological samples per condition; unpaired Mann-Whitney tests). **c,** Cholesterol accumulation in MCF10ATk1 cells transfected with SREBP1/2 siRNA (siSREBP mixes A and B) and plated on soft hydrogels. Scale bar 5µm. Quantification and n is provided in Supplementary Table 2. **d,** Immunofluorescence for endogenous SREBP2 in MCF10ATk1 cells with inhibited ROCK/MLCK (YM), RHO (C3 plasmid transfection), MyosinII (Blebbistatin 10µM), or plated on soft hydrogels for 6 hours. Cell contour in the YM 2h panel (dotted line) helps visualizing SREBP2 concentration at the Golgi apparatus. Scale bar 10µm. n>50 cells per condition. **e,** Western blotting for the mature form of endogenous SREBP1 and SREBP2 in MCF10ATk1 cells treated 4 hours with YM or FM. TEAD1 is a loading control for nuclear extracts. See also Supplementary Fig. 8. **f,** Immunofluorescence for endogenous SREBP2 in MCF10ATk1 cells treated 4 hours with YM in the presence of 100µg/ml cycloheximide (CHX). Scale bar 10µm. n>50 cells per condition. **g,** Western blotting on total extracts of MCF10ATk1 cells untreated (-), treated for 3 hours with 2µg/ml puromycin alone (puro) or with puromycin and 100µg/ml cycloheximide (CHX). Incorporation of the puromycin aminoacid analog into nascent proteins is used as control for efficient inhibition of protein synthesis. See also Supplementary Fig. 8. **h,** *LDLR-luciferase* in MDA231 cells. YM and FM activate endogenous SREBP, but have no additive effects in cells depleted of SREBP1/2 (siSREBP) and expressing a siRNA-insensitive, cleaved mature SREBP2 cDNA (caSREBP2). Mean expression in controls was set to 1, and other samples are relative to this (n≥4 independent biological samples per condition; unpaired Mann-Whitney tests). **i,** Heatmap of SREBP and YAP target levels in n=7 patient-matched soft normal skin vs. stiff keloid tissue. Each column represents -log2(keloid/skin) values for a single patient; each line is a single gene probe; genes ranked according to expression in patient #1. Selected gene names are indicated on the right; only the 60 most up- or downregulated genes (P<0.05) are included. All n values are pooled between independent experiments. The images in **c-g** are representative of at least two independent experiments with similar results. Data are mean and single points.

Figure 4. ECM mechanical cues regulate SCAP accumulation to the Golgi apparatus.
a, Co-localization of transfected MYC-tagged SCAP with a Golgi marker (GM130) in MCF10ATk1 cells cultured 6 hours on soft hydrogels (E≈0.5kPa), treated 6 hours with Y27632+ML7 (YM) or transfected with the C3 RHO inhibitor. Scale bar 10µm. n>50 cells per condition. **b,** Co-localization of transfected MYC-SCAP with a Golgi marker (GFP-Rab6) in RPE1 cells treated 6 hours with YM. Scale bar 10µm. n>50 cells per condition. **c,** *LDLR-luciferase* in MDA231 cells transfected with control siRNA (siCo.), with two independent SCAP siRNA (siSCAP A and B), or treated with 30µM 25-hydroxycholesterol (25OHC). **d,** *LDLR-luciferase* in MDA231 cells treated with the site-1 protease (S1P) inhibitor PF429242 (10µM). **e,** *LDLR-luciferase* in MDA231 cells transfected the C3 RHO inhibitor and treated as in **c** and **d**. In panels **c-e,** n≥4 independent biological samples per condition; mean expression in controls were set to 1, and all other samples are relative to this; data are mean and single points; unpaired Mann-Whitney tests. **f,** Human Pluripotent Stem Cells (hPSC) were dissociated and plated as single cells in the absence (DMSO) or presence of 10µM Y27632, without or with titrated doses of Cerivastatin (Ceri 25nM) and TOFA (75nM) for 24 hours, released in medium without inhibitors for 4 days, and stained for alkaline phosphatase to visualize self-renewing colonies. Lower panels: similar treatment on already-established colonies. Higher doses of Ceri/TOFA (10µM and

15μM) inhibit also established colonies. **g,** hPSC plated as in **f** and treated with 1,25μM 25-hydroxycholesterol. **h,** hPSC transfected with the indicated siRNAs and plated as single cells. The images in **f-h** are representative of at least two independent experiments with similar results; quantifications and n are provided in Supplementary Table 2. All n values are pooled between independent experiments.

Figure 5. ECM mechanical cues regulate Lipin-1/ARF1 signaling.

a,b, qPCR for SREBP target genes in MCF10ATk1 cells treated with DMSO or with 100μM Propranolol (Propra) to inhibit Lipin-1 phosphatidate phosphatase activity (**a**), or transfected with control (siCo.) and Lipin-1 siRNA (siLipin-1) (**b**). Data are relative to *GAPDH* levels; mean expression in controls was set to 1, and all other samples are relative to this (n≥4 independent biological samples per condition; multiple unpaired Student's t-tests). **c,** *LDLR-luciferase* in MDA231 cells transfected with the indicated siRNA and treated with 100μM Propranolol (Propra). Mean expression in the control was set to 1, and all other samples are relative to this (n≥4 independent biological samples per condition; unpaired Mann-Whitney tests). **d,** Immunofluorescence for endogenous SREBP2 in MCF10ATk1 cells treated with Propranolol, transfected with Lipin-1 or COPI siRNA, or expressing dominant-negative ARF1-T31N-GFP (DN ARF1). Scale bar 10μm. n>50 cells per condition. **e,** Co-localization of transfected MYC-SCAP with the GFP-Rab6 Golgi marker in RPE1 cells treated 6 hours with Propranolol, in cells transfected with control (siCo.), Lipin-1 or COPI siRNAs, or expressing dominant-negative ARF1-T31N (DN ARF1). Scale bar 10μm. n>50 cells per condition. **f,** Lipid staining in MCF10ATk1 cells treated for 24 hours with YM, with 100μM Propranolol, or transfected with Lipin-1 siRNA. Scale bar 5μm. Quantifications and n are provided in Supplementary Table 2. **g,** Western blotting for Lipin-1 levels in microsomal fractions from MCF10ATk1 cells treated 3 hours with DMSO or Y27632+ML7 (YM). Calreticulin (ER marker) and GM130 (Golgi marker) are loading controls. See also Supplementary Fig. 8. **h,** Co-localization of transfected GFP-PKD-KD with the GM130 Golgi marker in HEK293 cells treated for 30 min with YM, with 100μM Propranolol, or transfected with control (siCo.) and Lipin-1 siRNAs. Scale bar 10μm. Mean Pearson's correlation coefficient and SD for co-localization is indicated above each panel (n≥10 cells were measured for each condition). **i,** GST-GGA3-PBD pulldown for GTP-bound active ARF1 (GTP-Arf1) and western blotting for ARF1 in the total extracts (Total Arf1). Cells were treated 3 hours with DMSO or YM. See also Supplementary Fig. 8. **j,** Co-localization of endogenous ARF1 with a Golgi marker (GM130) in MCF10ATk1 cells treated 6 hours with YM or Propranolol. Scale bar 10μm. Mean Pearson's correlation coefficient and SD for co-localization is indicated above each panel (n≥10 cells were measured for each condition). The images in **d-j** are representative of at least two independent experiments with similar results. All n values are pooled between independent experiments. Data are mean and single points.

Figure 6. Actomyosin contractility regulates SREBP through Lipin-1.

a, Western blotting for transfected FLAG-tagged Lipin-1 in HEK293 cells treated with DMSO or YM for 6 hours. The 17S/A mutant is not phosphorylated and migrates faster than WT Lipin-1. GAPDH serves as loading control. See also Supplementary Fig. 8. **b,** Immunofluorescence for transfected FLAG-Lipin-1 in MCF10ATk1 cells treated 6 hours with YM, Blebbistatin, or plated on a soft hydrogel. Scale bar 10μm. n>50 cells per condition. **c,** Immunofluorescence for transfected wild-type (WT) or 17S/A FLAG-tagged Lipin-1 isoforms in RPE1 cells, treated with DMSO, YM or Torin1 (500nM) for 6 hours. Fusion with the membrane-localization domain of Syntaxin5 tethers MB-Lipin-1 to cytoplasmic membranes. Scale bar 10μm. n>50 cells per condition. Similar results were obtained

with MB*-Lipin-1 (used in **d**) and in other cell lines. **d,** *LDLR-luciferase* (top) and *FASN-luciferase* (bottom) assays in MDA231 cells treated with the ROCK/MLCK inhibitor FM and transfected with wild-type (WT), membrane-tethered (MB and MB*) or 17S/A Lipin-1 isoforms. **e,** *LDLR-luciferase* (top) and *FASN-luciferase* (bottom) assays in MDA231 cells transfected with the C3 RHO inhibitor without or with membrane-tethered (MB) Lipin-1. In **d** and **e**, mean expression in the control was set to 1, and all other samples are relative to this; n≥4 independent biological samples per condition; unpaired Mann-Whitney tests. **f,** MDA231 cells were transfected with WT-Lipin-1 or MB-Lipin-1 together with mCherry (RFP), treated with YM, and stained for cholesterol. n>30 cells per condition. Graph: cells were scored positive (+ve) for Filipin based on the presence/absence of cytoplasmic cholesterol accumulation. The images in **a, b, c** and **f** are representative of at least two independent experiments with similar results. All n values are pooled between independent experiments. Data are mean and single points.

Figure 7. The Golgi apparatus responds to extracellular physical cues and intracellular force application.

a, Co-localization of transfected MYC- SCAP with the GFP-Rab6 Golgi marker in RPE1 cells freely spreading on fibronectin-coated glass (Large) or plated on micropatterned fibronectin islands restraining cell area and inducing low F-actin tension (Small, 960μm^2 or 490μm^2). Scale bar 10μm. n>30 cells per condition. **b,** Golgi rheology was measured in RPE1 cells plated as in **a**. GFP-Rab6-positive Golgi membranes were pushed towards a cytoplasmic bead immobilized by an optical trap in a series of five 0.5μm steps in 1 min (see Supplementary Fig. **7a** and Methods). The graph shows the averaged displacements of the bead during the first step (see Supplementary Fig. **7b** for the complete graph). Green line: large unconfined cells, conditions of high tension (n=39 cells). The Golgi microenvironment displays a visco-elastic behavior as the bead is first maximally displaced (Bead Step Amplitude), and then slowly relaxes back due to attraction from the optical trap. Orange and Red lines: micropatterned small ECM (n=28, 21 cells). Gray shadows: s.e.m. error bars. A smaller displacement and a faster relaxation of the bead indicate a lower rigidity of the Golgi apparatus. **c,** The Rigidity Index (RI) measures the friction opposed by the Golgi microenvironment on the bead, with lower values indicating a softer microenvironment. The Bead Step Amplitude corresponds to the average displacement of the bead after each step, with lower values indicating a softer microenvironment. The Ejection Frequency measures the relative frequency of experiments in which the bead falls off the optical trap, which is increased with the resisting friction forces applied on the bead by the Golgi. **d,** Time-lapse confocal images of a representative RPE1 cell transfected with the GFP-PKD-KD diacylglycerol sensor and with a Golgi-localized mCherry. A 2μm-diameter cytoplasmic bead (yellow dotted line) was immobilized by an optical trap in the proximity of the Golgi apparatus (t=0) and then pushed every 5 min. towards the Golgi (white arrow: direction of the compressive constraint). **e,** Normalized intensity of the PKD-KD signal before and after application of force (n=19 cells). In the control the bead was moved away from the Golgi towards the cytoplasm (n=18 cells). The images in **a** and **d** are representative of at least two independent experiments with similar results. All n values are pooled between independent experiments. Data are mean and s.e.m.; two-tailed unpaired Student's t-tests.

Methods

Reagents. Plasmids encoding for SCAP-MYC, HA-S1P, HA-S2P were from Y. Chen (SIBS Shanghai), Perilipin3-RFP from L. Scorrano (UniPd), kinase-dead GFP-PKD1-K612W from A. Hausser (UniStuttgart), ARF1-T31N-GFP from A. DeMatteis (TIGEM Naples), KDEL-mCherry from E. Greotti (UniPd), GFP-OSBP from N. Ridgway (UniGlasgow). Addgene plasmids: FASN-lux #8890; LDLR-lux #14940; 8XGTIIC-lux #34615; NF2 #19701; CMV-Luc2P_ARE #62857; constitutive-active FLAG-SREBP2 #26807; FLAG-Lipin-1 WT #32005 and 17S/A #32007; mCherry-Golgi(B4GALT1) #55052. Full length SREBP1 and SREBP2 were subcloned from Addgene plasmids #32017 and #32018. ER/Golgi membrane-tethered Lipin-1 isoforms were obtained by in-frame fusion of the Syntaxin5 delta220 or TMD fragments[53,54] to FLAG-Lipin-1 WT and have been deposited as Addgene plasmids #120277 and #120278. SUMOylation (K616/646A) and acetylation (K476/646A) FLAG-Lipin-1 mutants were obtained by targeted mutagenesis. All plasmids were sequence-verified before use and transfected as endotoxin-free maxi preps.

Small molecule inhibitors were: Y27632 (Axon 1683, 20 microM, 10 microM on hPSC); Fasudil/HA1077 (SantaCruzBiotechnology sc358231, 20 microM); ML7 (Sigma I2764, 20 microM); Blebbistatin (Sigma B0560, 20 microM); Propranolol (Sigma P0884, 100 microM); Cycloheximide (Sigma C1988, 100 microg/ml); TOFA (Sigma T6575, 15 microM, 75 nanoM on hPSC); Cerivastatin (Sigma SML0005, 10 microM, 25 nanoM on hPSC); 25-hydroxy-cholesterol (Sigma SML2042, 30 microM, 1.25 microM on hPSC); U18666A (SantaCruzBioTechnology sc203306, 3 microM); PF429242 (Sigma SML0667, 10 microM); Z-VAD-FMK (Sigma V116, 30 microM); Torin1 (Axon 1833, 500 nanoM); MG132 (Sigma C2211, 10 microM); MG115 (Sigma C6706, 10 microM).

siRNAs were selected among FlexiTube GeneSolution 4 siRNA sets (Qiagen) and reordered after validation as dTdT-overhanging 19nt RNA duplexes (Thermo). siRNA sequences: SREBF1a CGGAGAAGCUGCCUAUCAA; SREBF1b GCGCACUGCUGUCCACAAA; SREBF1c GCGCACUGCUGUCCACAAA; SREBF1d ACAGCAACCAGAAACTCAA; SREBF2a GCAGUGUCCUGUCAUUCGA; SREBF2b GCAAUUUGUCAGUAAUCAA; SREBF2c GGCCAUUGAUUACAUCAAA; SREBF2d CGAUAUCGCUCCUCCAUCA; SCAPa GGAAGAUCGACAUGGUCAA; SCAPb GGCCGACGCUCUUCAGCUA; LPIN1 GUUCGGAUACCUUCAGUAA; YAP CUGGUCAGAGAUACUUCUU; TAZ AGGUACUUCCUCAAUCACA; AMPKa1/2 mixes a and b see Ref.[55]; COPIa GAUUUACCGAGGAGCAUUA; COPIb GGAUCGCUUGAUAGAAUUA; AllStars Negative Control (Qiagen) sequence not available – proprietary information.

Cell cultures. MCF10A, MCF10ATk1 MCF10ATk1 pBABE mTAZ 4SA were cultured in DMEM/F12 5%HS Insulin (Sigma) Cholera Toxin (Sigma) hEGF (Peprotech) and Hydrocortisone (Sigma). GFP-Rab6 and parental RPE1 in DMEM/F12 10%FBS (neomycin for GFP-Rab6). MDA-MB-231 in DMEM/F12 10%FBS. HEK293 in DMEM 10%FBS. WI-38 in MEM 10%FBS 5% oxygen. 3T3-L1 in DMEM 10%FBS 5% oxygen. H9 hPSC in E8 medium (DMEM/F12, NaHCO3, Insulin, Selenium, Transferrin, L-ascorbic acid, FGF2, TGFb1) 5% oxygen. WT and AMPKa1/2-/- MEFs in DMEM 20%FBS. Glutamine was freshly added to a final concentration of 20mM to all media. General media, serum and supplements were from Thermo. Cytokines from Sigma and Peprotech. All cell lines were routinely tested with ATCC Universal Mycoplasma Detection kit to exclude contaminations. Cells for immunofluorescence in a stiff microenvironment were plated on fibronectin-coated glass coverslips. Stiff (E≈15KPa) and soft (E≈0.5KPa) fibronectin-coated polyacrylamide hydrogels were assembled in-house by standard protocols. Annular-shaped micropatterns (25 or 35μm diameter, 5μm line thickness) were printed on PEG-coated glass coverslips by deep UV photolithography and coated with 50μg/ml fibronectin supplemented with 20μg/ml Alexa647-fibrinogen (Sigma). hPSC were

dissociated with Tryple (Thermo) and plated as single cells (2500 cells/2cm^2 well) in the presence or absence of the indicated small molecules for 24 hours; medium was then changed and cells were left growing for 4-5 days, until the appearance of macroscopic colonies. Treatment of colonies was done on colonies grown from single cells as above, and then treating for 24 hours. Cell transfections were carried out with Transit-LT1 (MirusBio) or with Lipofectamine RNAi-MAX (Thermo).

Antibodies, immunofluorescence and stains. See Supplementary Table 1 for catalog numbers, dilutions and validations. For the SREBP2 antibodies, independent lots were used with consistent results. Immunofluorescence was performed as in[56] with minor modifications: 10min 1.5mg/ml glycine in PBS before permeabilization to reduce background; blocking in 1-2% BSA. Images were acquired sequentially with a Zeiss LSN700 or a Leica SP5 confocal microscope equipped with a CCD camera using ZEN 2 or Leica LAS AF softwares. Typical acquisition settings for IF were: image size 1024x1024 pixels; acquisition mode xyz; pixel size 0.15µm; image depth 8 bits; acquisition speed 5/10, with average 2; Plan-Apochromat 63x/1.40 oil DIC M27 objective. For multichannel acquisitions, we used a main beam splitter 405/488/555/639. Raw images (saved in .czi or .lif formats) were opened in ImageJ and saved in exportable formats. If needed, colors were changed (e.g. red to green) with Photoshop CC.

Oil Red-O staining (Sigma) was carried out after fixation, in 60% v/v isopropanol/water. C11-Bodipy581/591 (Thermo) were incubated 15min with cells before FACS analysis. Filipin staining was acquired using a UV filter set (340/380nm excitation, 40nm dichroic, 430nm long pass filter) by prefocusing cells based on TOTO3 nuclear counterstain (633/647nm) and then acquiring the UV channel without prior observation to avoid photobleaching. Typical acquisition settings for Filipin were: image size 1024x1024 pixels; acquisition mode xyz; pixel size 0.15µm; image depth 8 bits; acquisition speed 5/10, with average 2; Plan-Apochromat 63x/1.40 oil DIC M27 objective. Pictures were always taken by using the same acquisition conditions between all different experimental samples; panels are representative pictures based on at least two independent experiments. Quantifications and n are provided in Supplementary Table 2.

Alkaline phosphatase staining was Leukocyte AP kit (Sigma). Panels shown are representative pictures of one biological replicate of one experiment; each experiment was repeated three times independently. Quantifications and n are provided in Supplementary Table 2.

Cell fractionation, western blotting and pulldown. Nuclear extracts and microsomes were obtained by resuspending cells in lysis buffer (250mM Sucrose, 10mM Triethanolamine pH=7.4, 10mM AceticAcid, 1mM EDTA, 10mM KCl) and passing cells 8 times (i.e. complete lysis at the microscope) through an Isobiotec Cell Homogenizer with a 6micron clearance sphere. Lysates were centrifuged at 800rcf to isolate nuclei, and then at 100.000rcf to isolate microsomes. Western blotting was performed as in Ref[57]; in Fig. **3e** and Supplementary Fig. **3h** cells were incubated with 10microM MG132/MG115 proteasome inhibitors during treatment to prevent degradation of cleaved SREBPs. Active GTP-bound ARF1 pulldown was performed with a commercial kit following the manifacturer's intructions (Cytoskeleton Inc. BK032).

Gene expression studies. Luciferase assays were performed in MDA-MB-231 cells as in Ref.[55]. For qPCR, total RNA was isolated using commercial kits with DNAse treatment (Qiagen, Norgen). cDNA synthesis was carried out with M-MLV Reverse Trascriptase (Thermo) and oligo-dT primers. qPCR reactions were assembled with FastStart SYBR Green Master Mix (Roche) and run on a QuantStudio6 thermal cycler (Thermo). Gene expression levels for each biological sample was quantified as the mean between three technical replicates; *GAPDH* expression levels were used to normalize gene expression between samples, based on the $2^{-\Delta\Delta Ct}$ method.

Sequences of primers: *ACSS2* For GTT GAC TCC CCT TCC TGG TG, Rev CTT CCA ACT CTT CCC CGG AC; CTGF AGG AGT GGG TGT GTG ACG Rev ACC AGG CAG TTG GCT CTA ATC; *DHCR7* For CCG CCC AGC TCT ATA CCT TG, Rev ACT TGT TCA CAA CCC CTG CA; *FASN* For GGA GGA GTG TAA ACA GCG CT, Rev TTG GCA AAC ACA CCC TCC TT; *HMGCR* For TGC AGC AAA CAT TGT CAC CG, Rev CAC CAC CCA CCG TTC CTA TC; *HMGCS1* For ACA CAA GAT GCT ACA CCG GG, Rev ATG GGT GTC CTC TCT GAG CT; *LDLR* For AAG GAC ACA GCA CAC AAC CA, Rev AAA GGA AGA CGA GGA GCA CG; *LPN1* For ACA TGG ATC CTG AAG TGG CG, Rev GAG ATG GCG ATG GAA GGG AG; *SQLE* For AGG CGC AGA AAA GGA ACC AA, Rev GCC AGC TCC CAC GAT GAT AA; *SCD* For CCA CTT GCT GCA GGA CGA TA, Rev CCA AGT AGA GGG GCA TCG TC; *SREBF1* For CGT TTC TTC GTG GAT GGG GA, Rev CCC GGA ATA GCT GAG TCA CC; *SREBF2* For GGG CTG GTT TGA CTG GAT GA, Rev AGA TCT GCC TGT TTC CGG TG; *SCAP* For CAG CAG CAA CAC AGT GAC CT, Rev TAT GGT CTT GGC TCC CTG TC; *GAPDH* For CTC CTG CAC CAC CAA CTG CT, Rev GGG CCA TCC ACA GTC TTC TG; *COPI* For AGT ACA GCC TGA TGA CCC CA, Rev TGC TGC CTC TTT CCT CTG TG; *AMPKa1* For CTT GCC AAA GGA GTG ATT CAG ATG C, Rev AGG TCA ACA GGA GAA GAG TCA AGT GT; *AMPKa2* For AGC GTT CCT GTT CTG CTG CT, Rev TCC ATG GTG TGA CTG CCC AG.

Microarray probe synthesis, hybridization and detection were performed at CMB Trieste on HumanHT-12 v4 Expression BeadChips with an Illumina Hiscan system. Data analyses were performed in R (version 3.0.2) using Bioconductor libraries (BioC 2.13) and R statistical packages. Probe level signals were converted to expression values using robust multi-array average procedure RMA[58] of Bioconductor Affymetrix package. Differentially expressed genes were identified using Significance Analysis of Microarray (SAM) algorithm coded in the same R package[59]. In SAM, we estimated the percentage of false-positive predictions (i.e., false discovery rate, FDR) with 100 permutations. Genes activated or inhibited upon YM treatment and used for Gene List Enrichment Analysis were filtered based on *P*-value<0.05 and fold change>1.3. Gene List Enrichment Analysis was performed with Enrichr[60]. SREBP target genes were defined based on Ref.[61,62].

Metabolomics and metabolic analyses. Large-scale metabolic analysis (global metabolomics) and Principal Component Analysis of the results was carried out by Metabolon Inc. Mechanosensitive MCF10Tk1 cells[56] were washed once in warm 1XPBS, and metabolites were extracted 5 min at RT on 15cm plates with 80% v/v Methanol/Water extraction buffer with internal standards. We harvested cells on plate to specifically avoid alteration of actin tension and of metabolism due to cell detachment. Metabolites were normalized to protein content. This analysis did not focus on triglyceride content. Clustering of selected lipid metabolites (fold change>2.5; p-value<0.05) shown in Supplementary Fig. **1e** was carried out with Heatmapper.

Targeted lipidomic analysis was carried out on MCF10Tk1 cells lysed in 1:1 v/v MeOH/Acetonitrile extraction buffer by tissue lyser and spun at 20,000g for 5 min at 4°C. Supernatant were then passed through a regenerated cellulose filter, dried and resuspended in 100µl of MeOH.

For the quantification of the different phospholipid species the liquid chromatography tandem mass spectrometry LC-MS/MS analysis was performed on API-4000 triple quadrupole mass spectrometer (AB Sciex) coupled with a HPLC system (Agilent) and CTC PAL HTS autosampler (PAL System). The identity of the different phospholipid families was confirmed using pure standards, namely one for each family. Methanolic extracts were analyzed by a 5 minutes run in both positive and negative ion mode with a 275 multiple reaction monitoring (MRM) transitions in positive mode and 92 MRM transitions in negative mode. Quantification of different phospholipids in positive ion mode was performed using a Synergi 4µ Hydro-RP (50mm x 2.0mm, 4µm; Phenomenex) and in negative ion mode using Cyano-phase LUNA column (50mm x 4.6mm, 5µm; Phenomenex). The mobile phase for

positive ion mode was 0.1 % formic acid in MeOH and 5 mM ammonium acetate pH 7 in MeOH for negative ion mode both with a with a flow rate of 500µl/min. MultiQuant™ software version 3.0.2 was used for data analysis and peak review of chromatograms. Semi-quantitative evaluation of different phospholipids was performed based on external standards, then data were normalized on protein content assessed by BCA method.

For the quantification of the different diacylglycerol and triacylglycerol species the liquid chromatography tandem mass spectrometry LC-MS/MS analysis was performed on API-4000 triple quadrupole mass spectrometer (AB Sciex) coupled with a HPLC system (Agilent) and CTC PAL HTS autosampler (PAL System). Methanolic extracts were dried under nitrogen and resuspended in 100µl of 65% Acetonitrile/30% isopropanol/5% water. Samples were then analyzed by a 10 minutes run in positive ion mode with a 92 multiple reaction monitoring (MRM) transitions. Quantification of different diacylglycerols and triacylglycerols was performed using a XBridge™ C-18 (100mm x 2.1mm, 3.5µm; Waters). Column temperature was set at 55°C. The mobile phases were phase A: 40% acetonitrile, 0.1 % formic acid and 10 mM ammonium acetate in water; phase B: isopropanol 90%, acetonitrile 10%, 0.1 % formic acid and 10 mM ammonium acetate. T_0: 55%A; T_{2min}: 55%A; T_{4min}: 3%A; T_{7min}: 3%A; $T_{7.1min}$: 55%A; T_{10min}: 55%A; with a flow rate of 260µl/min. MultiQuant™ software version 3.0.2 was used for data analysis and peak review of chromatograms. Semi-quantitative evaluation of different diacylglycerols and triacylglycerols was performed based on external standards, then data were normalized on protein content assessed by BCA method.

For isotopolog analysis, cells were exposed to 2.5mM [$^{13}C_2$]acetate (Sigma 282014) for 24h. After removing media, cells were washed in ice-cold PBS. Lipid extraction was performed by adding 500µl of MeOH/ACN (1:1 v/v), and then 2.5ml of chloroform-MeOH (1:1, v/v). Total FAs were obtained by acid hydrolysis adding 1.25ml of HCl 1M and 1.25ml of MeOH. After leaving samples 1h in agitation at 210 rpm, 2.5ml of chloroform-water (1:1, v/v) were added to the mixture and the lower organic phase was collected, split, transferred into tubes, and dried under nitrogen flow. The residue was resuspended in MeOH/H_2O (1:1, v/v) and used for total FA analysis. Sample were analyzed by and API 4000 mass spectrometer (AB Sciex) coupled with a HPLC system (Agilent) and CTC PAL HTS autosampler (PAL System). The gradient (flow rate 0.5 ml/min) was as follows: T0: 20% A, T20: 1% A, T25: 1% A, T25.1: 20% A, T30: 20% A, where A: acetic acid 15mM and N-ethylisopropylamine 10mM in H_2O:MeOH 97:3 and B: MeOH. The Hypersil GOLD^{TM} column (C8 100mm x 3mm, 3µm; Thermo-Scientific) was maintained at 40°C for all the analysis.

For the quantification of free and total fatty acids and cholesterol levels, we used an aliquot of extracts described above and commercial kits (Sigma MAK044 and MAK043) following the instructions.

Intracellular optical micromanipulation, microrheological measurements and analysis. The set-up combining optical trapping and confocal imaging was described previously[47]. Briefly, red fluorescent 580/605nm 2µm diameter latex beads (Thermo F88265) were endocytosed overnight in RPE1 cells stably expressing the Golgi marker GFP-Rab6. The incubation time and bead concentration were adjusted so that cells typically contained one or two beads before optical micromanipulation. Cells were plated on 18mm diameter coverslips uniformly coated with fibronectin, or with annular-shaped adhesive fluorescent micropatterns of different diameters (25 or 35 µm), during 6 hours. Non-adherent cells were washed off by rinsing with culture medium. The coverslip was then mounted in a Ludin chamber and the culture medium was supplemented with 20mM Hepes prior to the experiment.

Force was applied on GFP-positive Golgi membranes by first trapping a bead located close to the Golgi apparatus and then displacing the microscope stage in order to push the organelle against the trapped bead. Trapping was not possible on polyacrilamide hydrogels because of the excessive distance

between lens and cells in this set-up. The applied force F was deduced from the bead displacement relative to the trap center Δx after calibration of the trap stiffness k_{trap} using $F = k_{trap}\ \Delta x$ with $k_{trap} = 280\ pN/\mu m$. The output power of the infra-red laser at the objective aperture was 150 mW. Stage displacement was performed using a nanopositioning piezo-stage (Nanobio 200, Mad City Labs) controlled by the NanoRoute3D software (Mad City Labs). The stage displacement consisted in five consecutive 0.5µm steps with a 10s pause between each step to allow visco-elastic relaxation of the bead position towards the trap center. The total duration of optical trapping was limited to 1 min for a given cell to ensure cell viability.

To characterize the rigidity of the microenvironment surrounding the bead, we used a phenomenological analysis of the relaxation curves as in[47,63] to measure three parameters: the frequency of bead ejection, the bead step amplitude and the rigidity index. Qualitatively, in a low rigidity microenvironment, friction on the bead is low and the bead does not move much from the trap center during the step displacement and relaxes rapidly towards the trap center. In a rigid microenvironment, the bead experiences a high friction and its initial displacement is bigger and closer to the step displacement (0.5µm) and the relaxation is slower. If the force acting on the bead is too large (typically above 300-400pN), the bead falls off the trap and subsequently follows the displacement of the stage. We termed such events 'ejections' and scored their frequency (defined as the ratio between the number of experiments in which ejection occurred and the total number of experiments) and the step at which ejection occurred. The bead step amplitude X_b corresponds to the displacement of the bead after a 0.5µm step of the piezo-stage. Values of X_b close to 0.5µm indicate a high rigidity of the bead microenvironment. Lower values are indicative of softer microenvironments. The rigidity index is defined as

$$RI = \frac{\int_{t_i}^{t_i+T} x_b(t)dt}{\int_{t_i}^{t_i+T} x_s(t)dt} = \frac{\int_{t_i}^{t_i+T} x_b(t)dt}{X_s T}$$

where t_i is the time when the i^{th} 0.5 µm step displacement of the piezo-stage occurs, x_b and x_s are respectively the displacement of the bead relative to the trap center and the displacement of the piezo-stage, $X_s = 0.5\mu m$ is the amplitude of the piezo-stage step and $T = 10s$ is the duration of the step. The rigidity index RI is a phenomenological parameter which allows us to compare the rigidity of the microenvironment surrounding the bead in various conditions. The value of RI falls between 0 (the microenvironment does not exert any friction on the bead) and 1 (the microenvironment is not deformable). The values of RI for each step displacement were averaged.

To measure GFP-PKD-KD recruitment upon force application, cells were plated at day 1 in a 12-well plate to reach around 75% confluence on day 2. At day 2, cells were transfected with GFP-PKD-KD and mCherry-Golgi(B4GALT1) plasmids. At the end of day 2, the cells were incubated with 2µm diameter fluorescent beads overnight. At day 3, cells were transferred to fibronectin-coated coverslips for the experiment. The evolution of normalized intensity of GFP-PKD-KD in the region of the Golgi apparatus, visualized by the mCherry-Golgi marker, was monitored after application of a mechanical constraint exerted by internalized beads trapped with optical tweezers. A bead located near the Golgi apparatus was selected in a cell expressing GFP-PKD-KD and the mCherry-Golgi marker. A first image was taken at t=0min. The bead was then trapped with the optical tweezers and the microscope stage manually displaced to bring the Golgi apparatus in contact with the bead and apply a compressive constraint on the Golgi apparatus during 1 min. The same protocol was repeated every 5min until t=30min. The duration of the compressive constraint was reduced to 30s after t=10min to avoid cellular damage due to prolonged laser exposure. As a control, the same protocol was used but the microscope stage was displaced in order to move the bead away from the Golgi apparatus.

To quantify the fluorescence intensity of GFP-PKD-KD in each of the seven images taken every 5 minutes, the Golgi apparatus was delimited using the mCherry Golgi marker. The total intensities of the mCherry Golgi marker (I_r) and of GFP-PKD-Kd (I_g) were measured as well as the mean intensity of the background for each channel ($\langle I_{r\,back}\rangle$ for the mCherry Golgi marker and $\langle I_{g\,back}\rangle$ for GFP-PKD-KD) and the area of the Golgi apparatus A_{Golgi}. The total intensity of the background in the Golgi apparatus region for each channel was then estimated by multiplying the mean background intensity by the Golgi area:

$$I_{r\,back} = A_{Golgi} \,.\, \langle I_{r\,back}\rangle$$
$$I_{g\,back} = A_{Golgi} \,.\, \langle I_{g\,back}\rangle$$

The fluorescence intensity of GFP-PKD-KD was normalized by the fluorescence intensity of the mCherry Golgi marker:

$$I = \frac{I_g - I_{g\,back}}{I_r - I_{r\,back}}$$

to account for slight changes in the imaging plane from one image to the next. The relative temporal variations of the GFP-PKD-KD fluorescence were obtained by normalizing the intensity I measured from each image taken every 5 minutes by its initial value I_0: $I(t) = I/I_0$.

Statistics and Reproducibility. All data are based on independent experiments with independent biological replicates, except for metabolomics and microarrays that were based on independent biological replicates harvested in a single experiment. Experimental repetitions were carried out by thawing a new aliquot of cells, deriving from the original stock. Key data were independently replicated by two different operators, across different cell lines, and with independent techniques providing coherent results. All n values are pooled between independent experiments. Data are presented as mean and single points, or mean and standard error of the mean (s.e.m.) as indicated in the figure legends. Significance tests were unpaired non-parametric Mann-Whitney tests, unpaired two-tailed Student's t-tests, multiple unpaired two-tailed Student's t-tests with Holm-Sidak correction (for analysis of multiple qPCR markers), or Welch's two sample t-tests (for global metabolomics). t-tests have been performed under the reasonable assumption that values follow a normal distribution and have similar variance.

Code availability

No custom codes were used in this study. All other codes are indicated in the appropriate methods sections and references.

Data availability. Microarray, metabolomics and targeted lipidomics data have been deposited (GEO database GSE107275 and Figshare database 10.6084/m9.figshare.7338764). Source data for Figs. **1-7** and Supplementary Figs. **1-7** have been provided in Supplementary Table **2**. All other data supporting the findings of this study are available from the corresponding author on reasonable request.

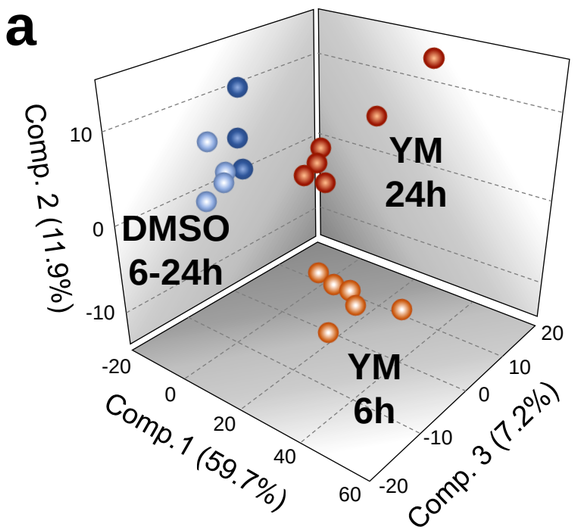
a
DMSO
6-24h
YM
24h
YM
6h
Comp. 2 (11.9%)
Comp. 1 (59.7%)
Comp. 3 (7.2%)

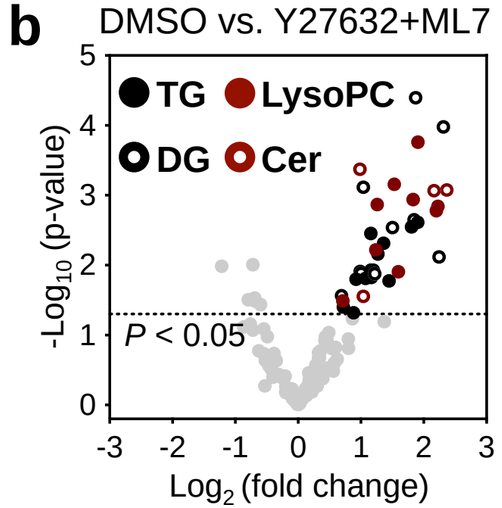
b
DMSO vs. Y27632+ML7
TG
LysoPC
DG
Cer
P < 0.05
-Log10 (p-value)
Log2 (fold change)

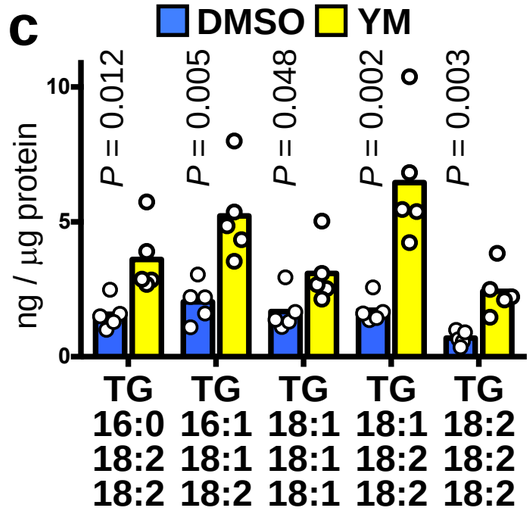
c
DMSO
YM
P = 0.012
P = 0.005
P = 0.048
P = 0.002
P = 0.003
ng / µg protein
TG 16:0 18:2 18:2
TG 16:1 18:1 18:2
TG 18:1 18:1 18:1
TG 18:1 18:2 18:2
TG 18:2 18:2 18:2

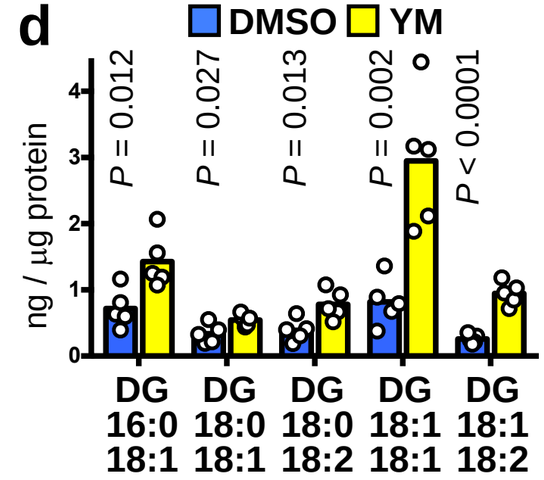
d
DMSO
YM
P = 0.012
P = 0.027
P = 0.013
P = 0.002
P < 0.0001
ng / µg protein
DG 16:0 18:1
DG 18:0 18:1
DG 18:0 18:2
DG 18:1 18:1
DG 18:1 18:2

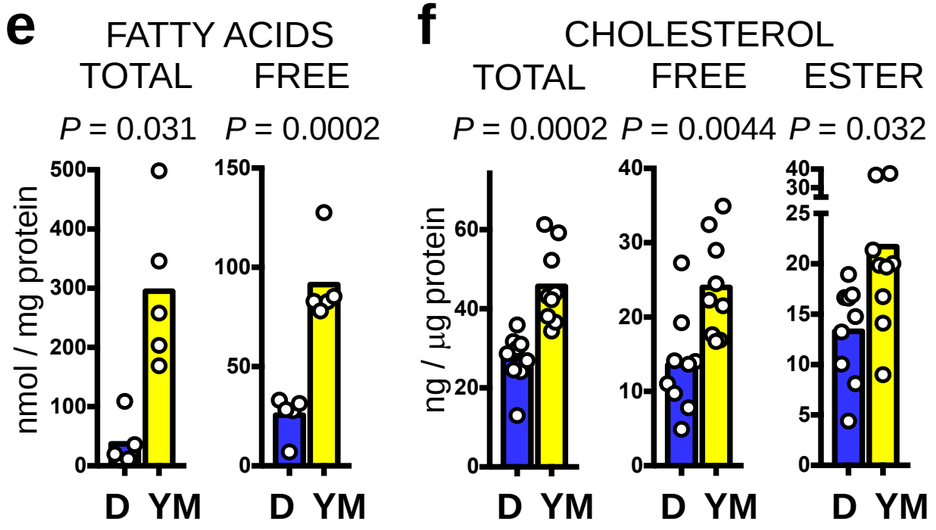
e
FATTY ACIDS
TOTAL
FREE
P = 0.031
P = 0.0002
nmol / mg protein
D
YM

f
CHOLESTEROL
TOTAL
FREE
ESTER
P = 0.0002
P = 0.0044
P = 0.032
ng / µg protein
D
YM

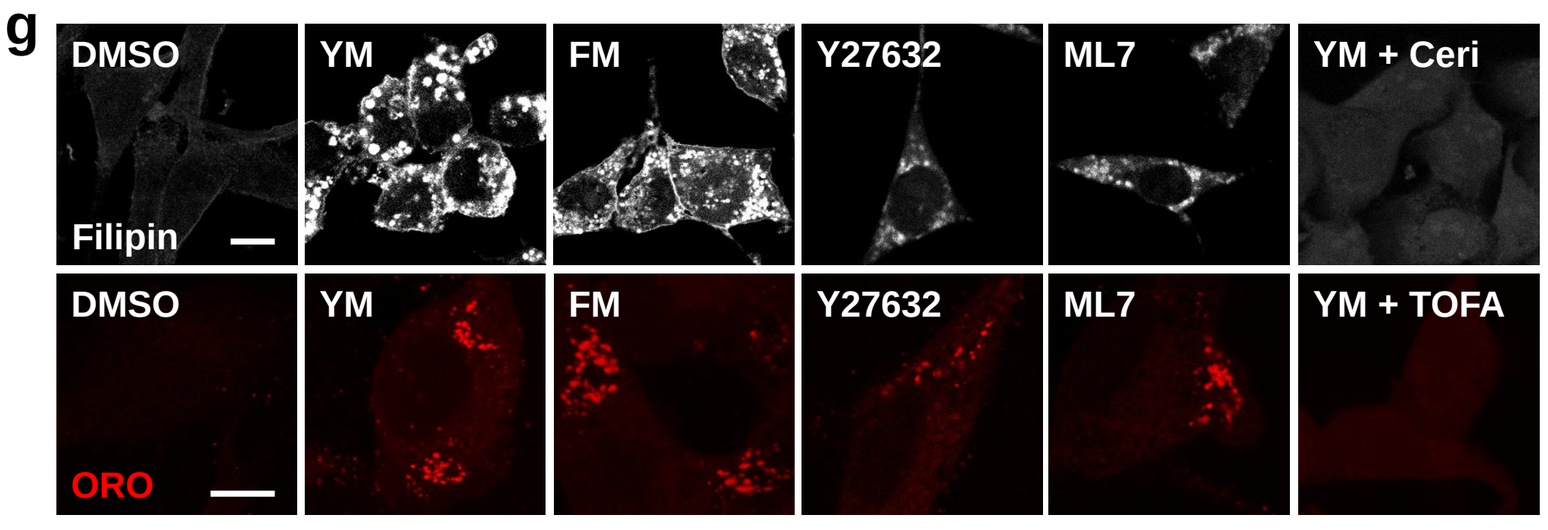
g
DMSO
YM
FM
Y27632
ML7
YM + Ceri
Filipin
DMSO
YM
FM
Y27632
ML7
YM + TOFA
ORO

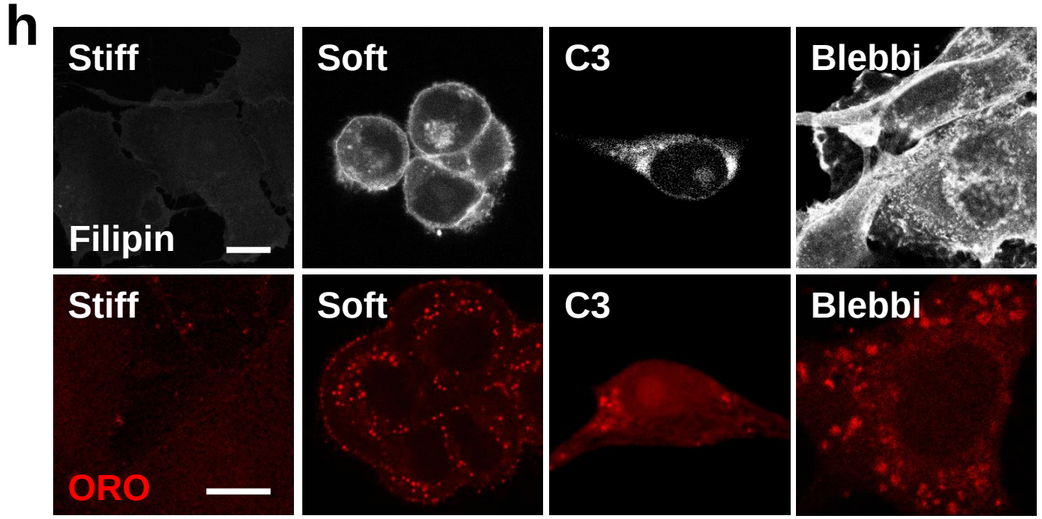
h
Stiff
Soft
C3
Blebbi
Filipin
Stiff
Soft
C3
Blebbi
ORO

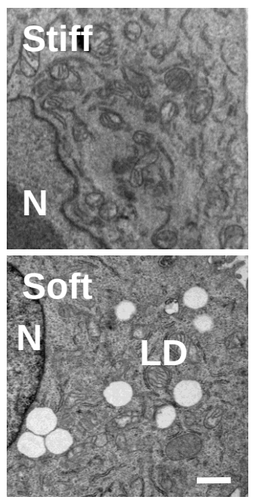
i
Stiff
N
Soft
N
LD

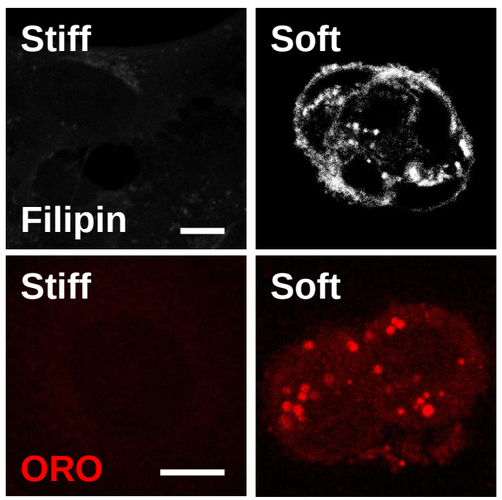
j
RPE1
Stiff
Soft
Filipin
Stiff
Soft
ORO

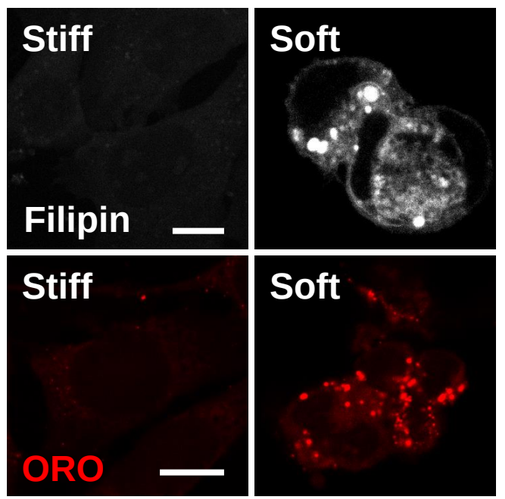
k
3T3L1
Stiff
Soft
Filipin
Stiff
Soft
ORO

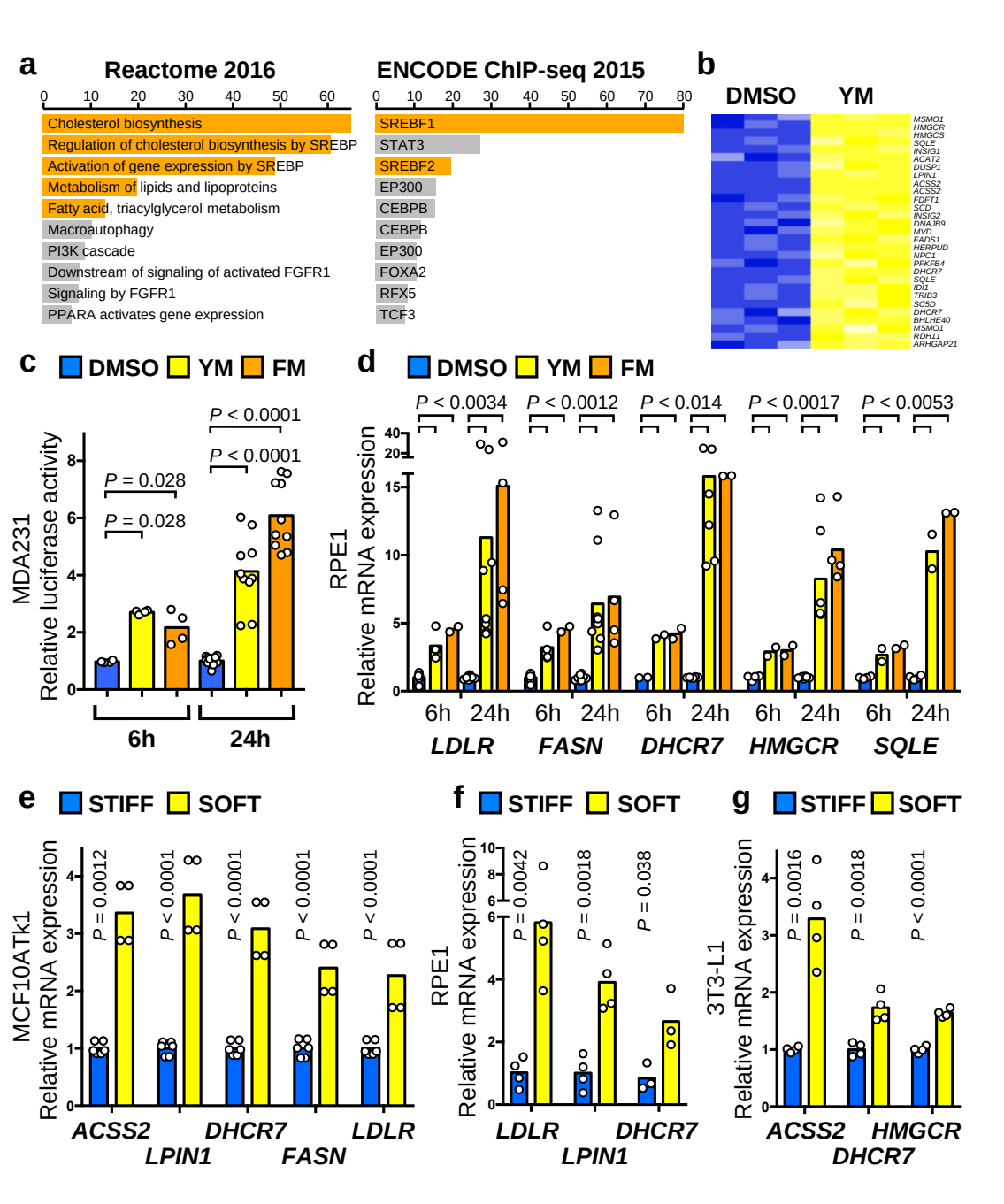
a
Reactome 2016
0 10 20 30 40 50 60
Cholesterol biosynthesis
Regulation of cholesterol biosynthesis by SREBP
Activation of gene expression by SREBP
Metabolism of lipids and lipoproteins
Fatty acid, triacylglycerol metabolism
Macroautophagy
PI3K cascade
Downstream of signaling of activated FGFR1
Signaling by FGFR1
PPARA activates gene expression
ENCODE ChIP-seq 2015
0 10 20 30 40 50 60 70 80
SREBF1
STAT3
SREBF2
EP300
CEBPB
CEBPB
EP300
FOXA2
RFX5
TCF3
b
DMSO
YM
MSMO1
HMGCR
HMGCS
SQLE
INSIG1
ACAT2
DUSP1
LPIN1
ACSS2
ACSS2
FDFT1
SCD
INSIG2
DNAJB9
MVD
FADS1
HERPUD
NPC1
PFKFB4
DHCR7
SQLE
IDI1
TRIB3
SC5D
DHCR7
BHLHE40
MSMO1
RDH11
ARHGAP21
c
DMSO YM FM
MDA231
Relative luciferase activity
P = 0.028
P = 0.028
P < 0.0001
P < 0.0001
6h
24h
d
DMSO YM FM
RPE1
Relative mRNA expression
P < 0.0034
P < 0.0012
P < 0.014
P < 0.0017
P < 0.0053
6h 24h 6h 24h 6h 24h 6h 24h 6h 24h
LDLR
FASN
DHCR7
HMGCR
SQLE
e
STIFF SOFT
MCF10ATk1
Relative mRNA expression
P = 0.0012
P < 0.0001
P < 0.0001
P < 0.0001
P < 0.0001
ACSS2
LPIN1
DHCR7
FASN
LDLR
f
STIFF SOFT
RPE1
Relative mRNA expression
P = 0.0042
P = 0.0018
P = 0.038
LDLR
LPIN1
DHCR7
g
STIFF SOFT
3T3-L1
Relative mRNA expression
P = 0.0016
P = 0.0018
P < 0.0001
ACSS2
DHCR7
HMGCR

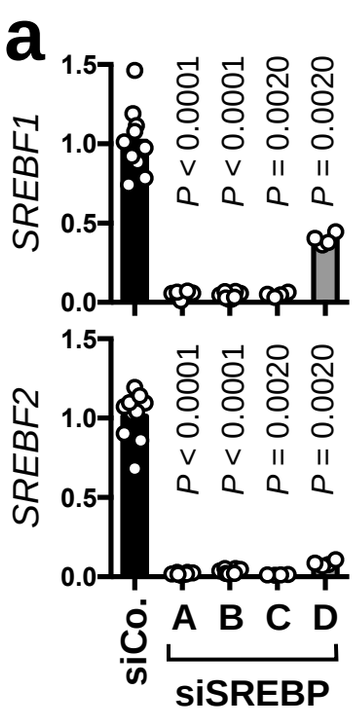
a
SREBF1
SREBF2
1.5
1.0
0.5
0.0
P < 0.0001
P < 0.0001
P = 0.0020
P = 0.0020
siCo.
A
B
C
D
siSREBP

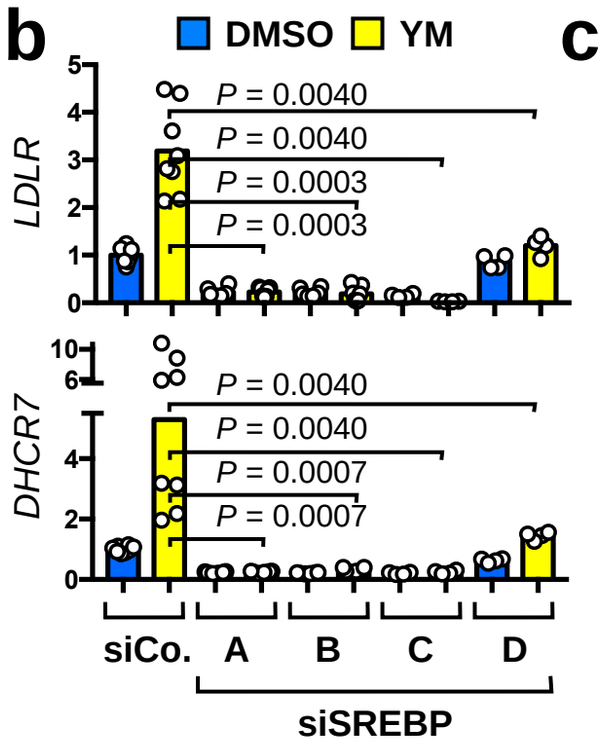
b
DMSO
YM
LDLR
DHCR7
P = 0.0040
P = 0.0040
P = 0.0003
P = 0.0003
P = 0.0040
P = 0.0040
P = 0.0007
P = 0.0007
siCo.
A
B
C
D
siSREBP

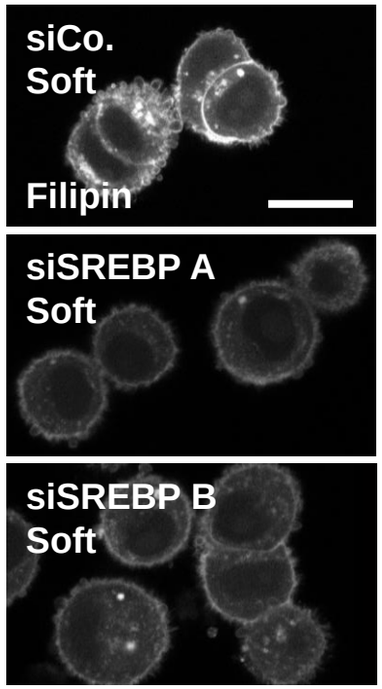
c
siCo.
Soft
Filipin
siSREBP A
Soft
siSREBP B
Soft

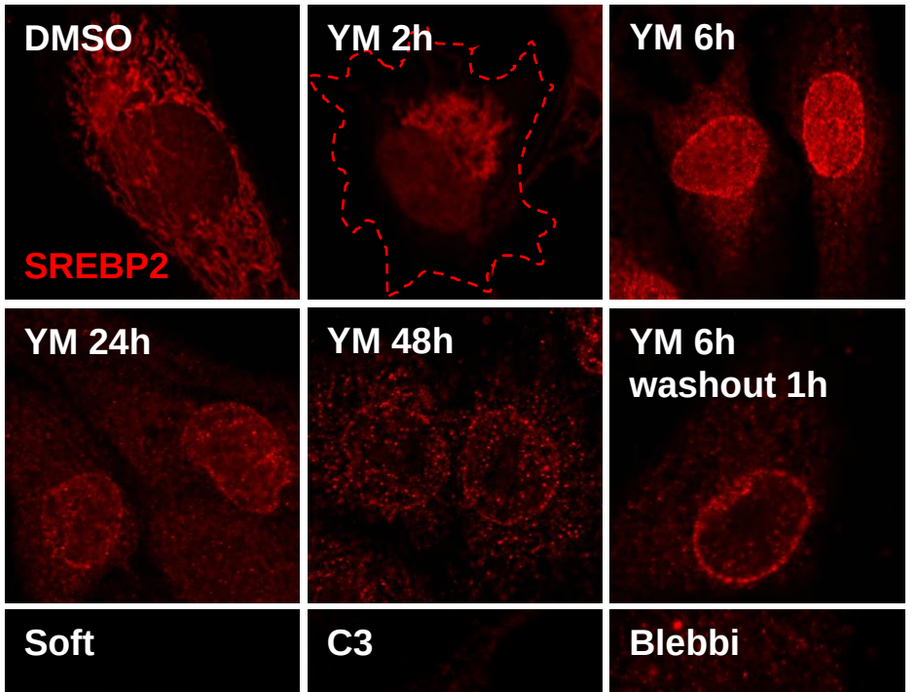
d
DMSO
SREBP2
YM 2h
YM 6h
YM 24h
YM 48h
YM 6h
washout 1h
Soft
C3
Blebbi

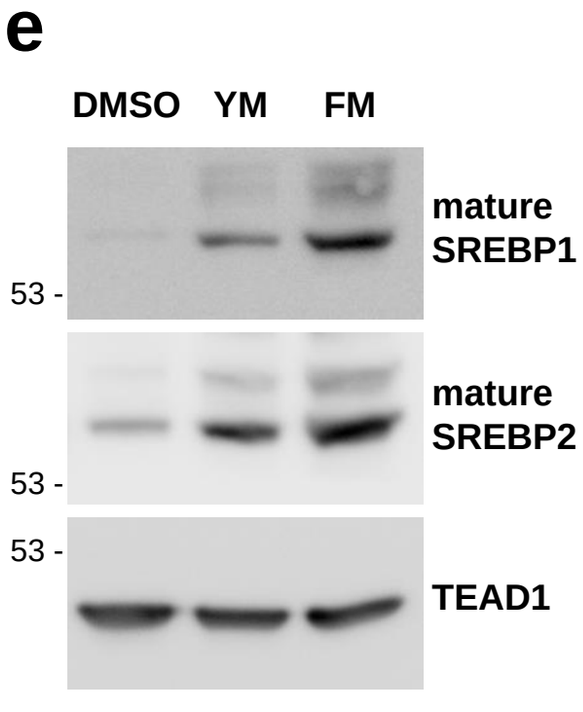
e
DMSO
YM
FM
53 -
mature
SREBP1
53 -
mature
SREBP2
53 -
TEAD1

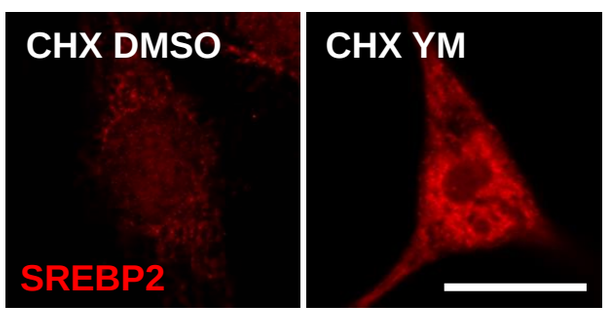
f
CHX DMSO
CHX YM
SREBP2

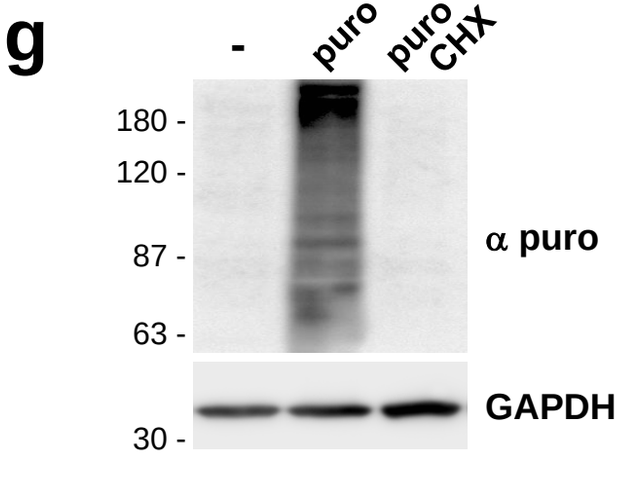
g
-
puro
puro
CHX
180 -
120 -
87 -
63 -
α puro
30 -
GAPDH

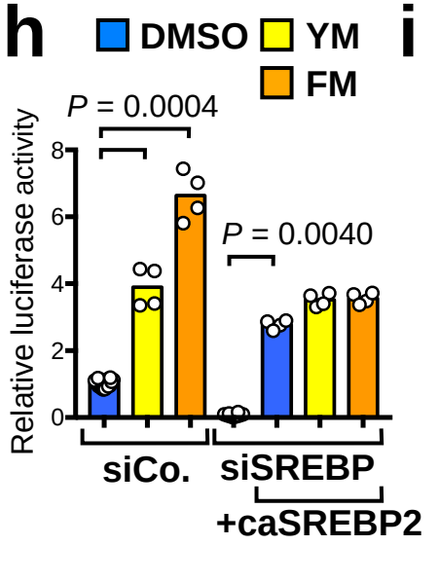
h
DMSO
YM
FM
P = 0.0004
P = 0.0040
Relative luciferase activity
siCo.
siSREBP
+caSREBP2

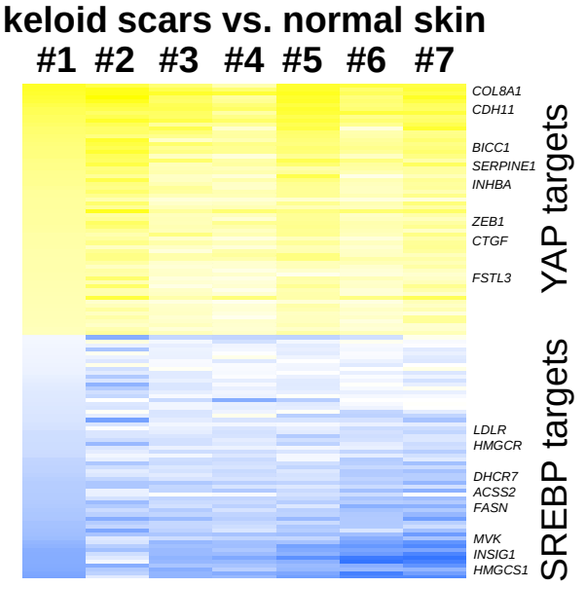
i
keloid scars vs. normal skin
#1
#2
#3
#4
#5
#6
#7
COL8A1
CDH11
BICC1
SERPINE1
INHBA
ZEB1
CTGF
FSTL3
YAP targets
LDLR
HMGCR
DHCR7
ACSS2
FASN
MVK
INSIG1
HMGCS1
SREBP targets

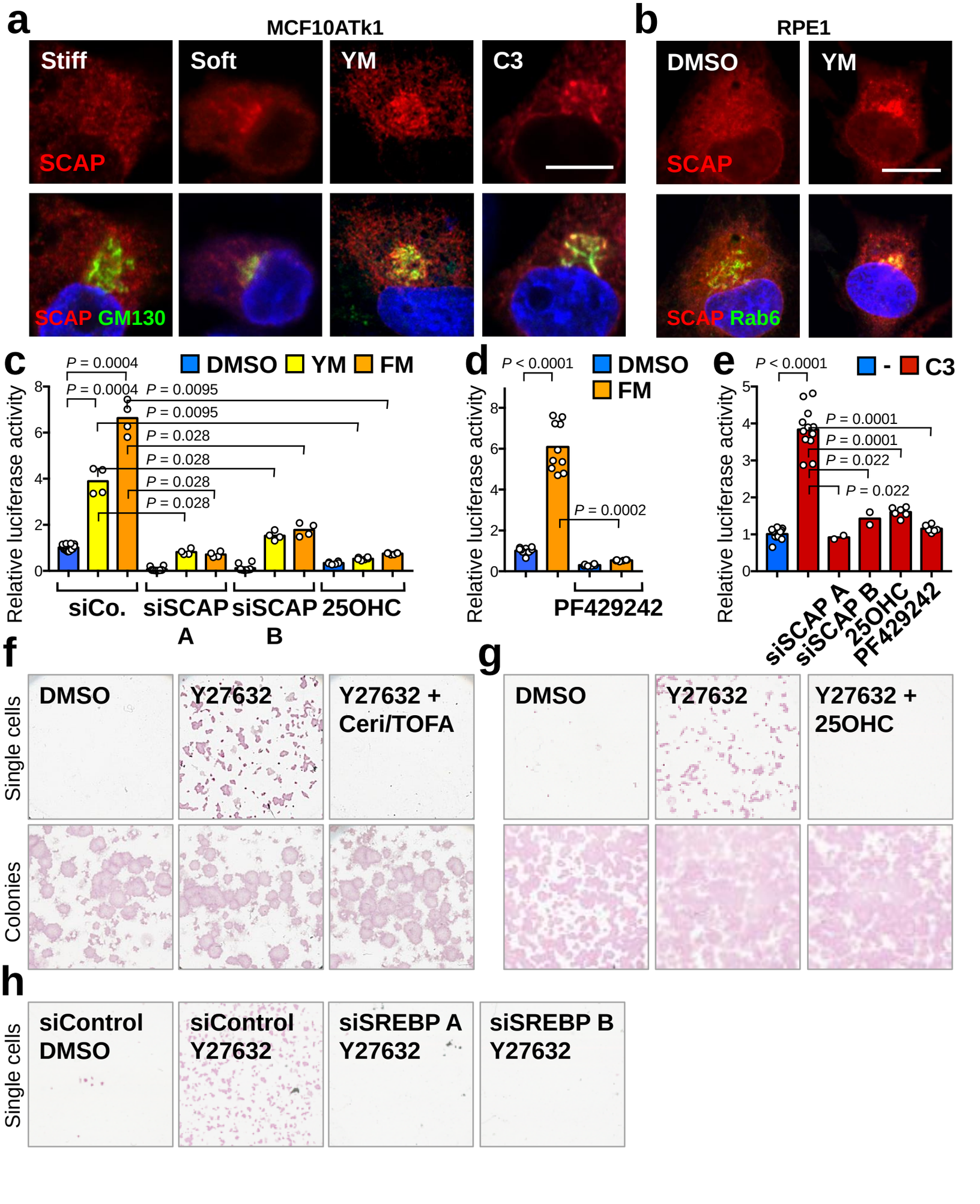
a
MCF10ATk1
Stiff
Soft
YM
C3
SCAP
SCAP GM130
b
RPE1
DMSO
YM
SCAP
SCAP Rab6
c
DMSO
YM
FM
Relative luciferase activity
P = 0.0004
P = 0.0004
P = 0.0095
P = 0.0095
P = 0.028
P = 0.028
P = 0.028
P = 0.028
siCo.
siSCAP A
siSCAP B
25OHC
d
P < 0.0001
DMSO
FM
P = 0.0002
PF429242
e
P < 0.0001
-
C3
P = 0.0001
P = 0.0001
P = 0.022
P = 0.022
siSCAP A
siSCAP B
25OHC
PF429242
f
Single cells
Colonies
DMSO
Y27632
Y27632 + Ceri/TOFA
g
DMSO
Y27632
Y27632 + 25OHC
h
Single cells
siControl DMSO
siControl Y27632
siSREBP A Y27632
siSREBP B Y27632

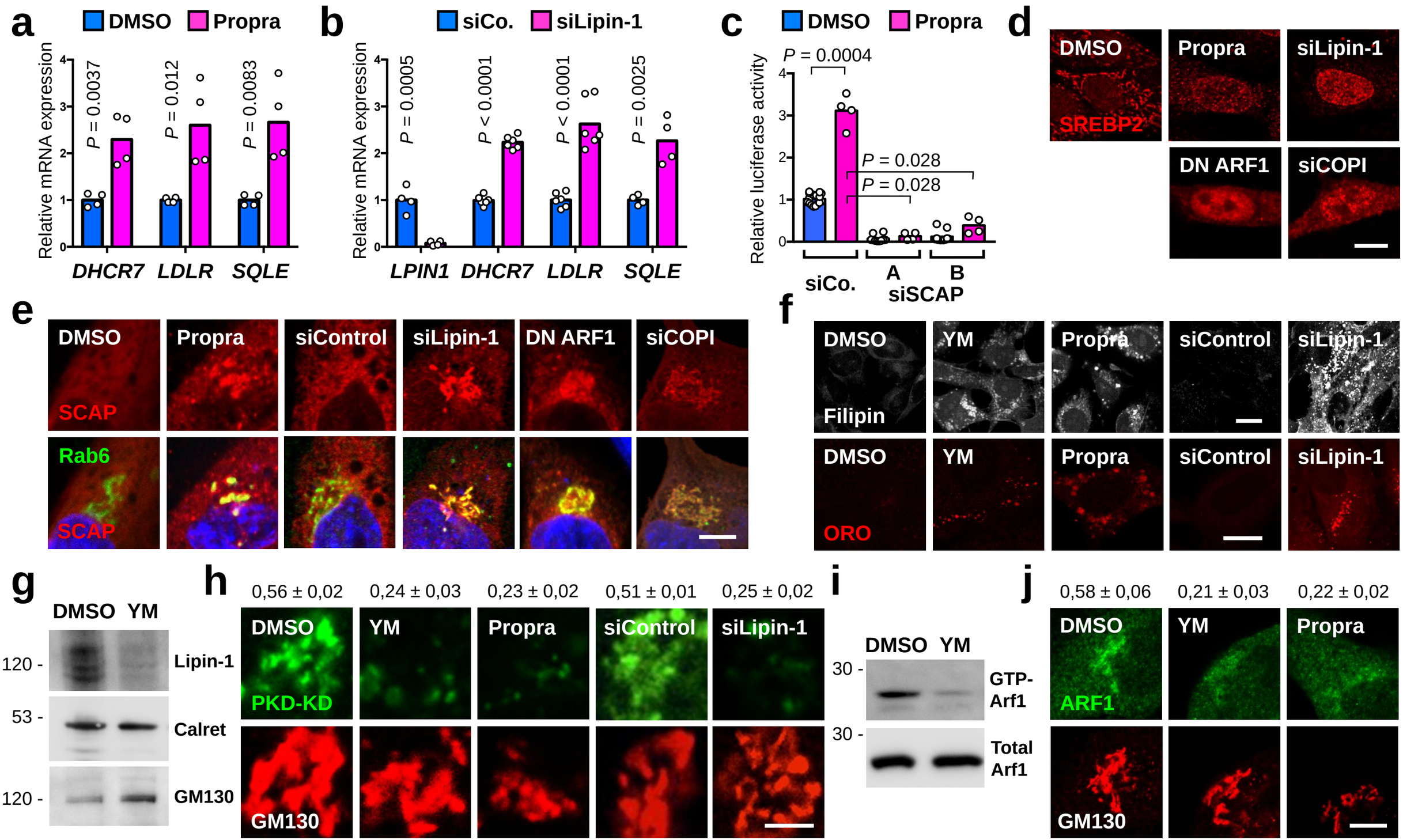
a
DMSO
Propra
Relative mRNA expression
P = 0.0037
P = 0.012
P = 0.0083
DHCR7
LDLR
SQLE
b
siCo.
siLipin-1
Relative mRNA expression
P = 0.0005
P < 0.0001
P < 0.0001
P = 0.0025
LPIN1
DHCR7
LDLR
SQLE
c
DMSO
Propra
Relative luciferase activity
P = 0.0004
P = 0.028
P = 0.028
siCo.
A
B
siSCAP
d
DMSO
SREBP2
Propra
siLipin-1
DN ARF1
siCOPI
e
DMSO
SCAP
Propra
siControl
siLipin-1
DN ARF1
siCOPI
Rab6
SCAP
f
DMSO
Filipin
YM
Propra
siControl
siLipin-1
DMSO
ORO
YM
Propra
siControl
siLipin-1
g
DMSO
YM
120 -
Lipin-1
53 -
Calret
120 -
GM130
h
0,56 ± 0,02
0,24 ± 0,03
0,23 ± 0,02
0,51 ± 0,01
0,25 ± 0,02
DMSO
PKD-KD
YM
Propra
siControl
siLipin-1
GM130
i
DMSO
YM
30 -
GTP-Arf1
30 -
Total Arf1
j
0,58 ± 0,06
0,21 ± 0,03
0,22 ± 0,02
DMSO
ARF1
YM
Propra
GM130

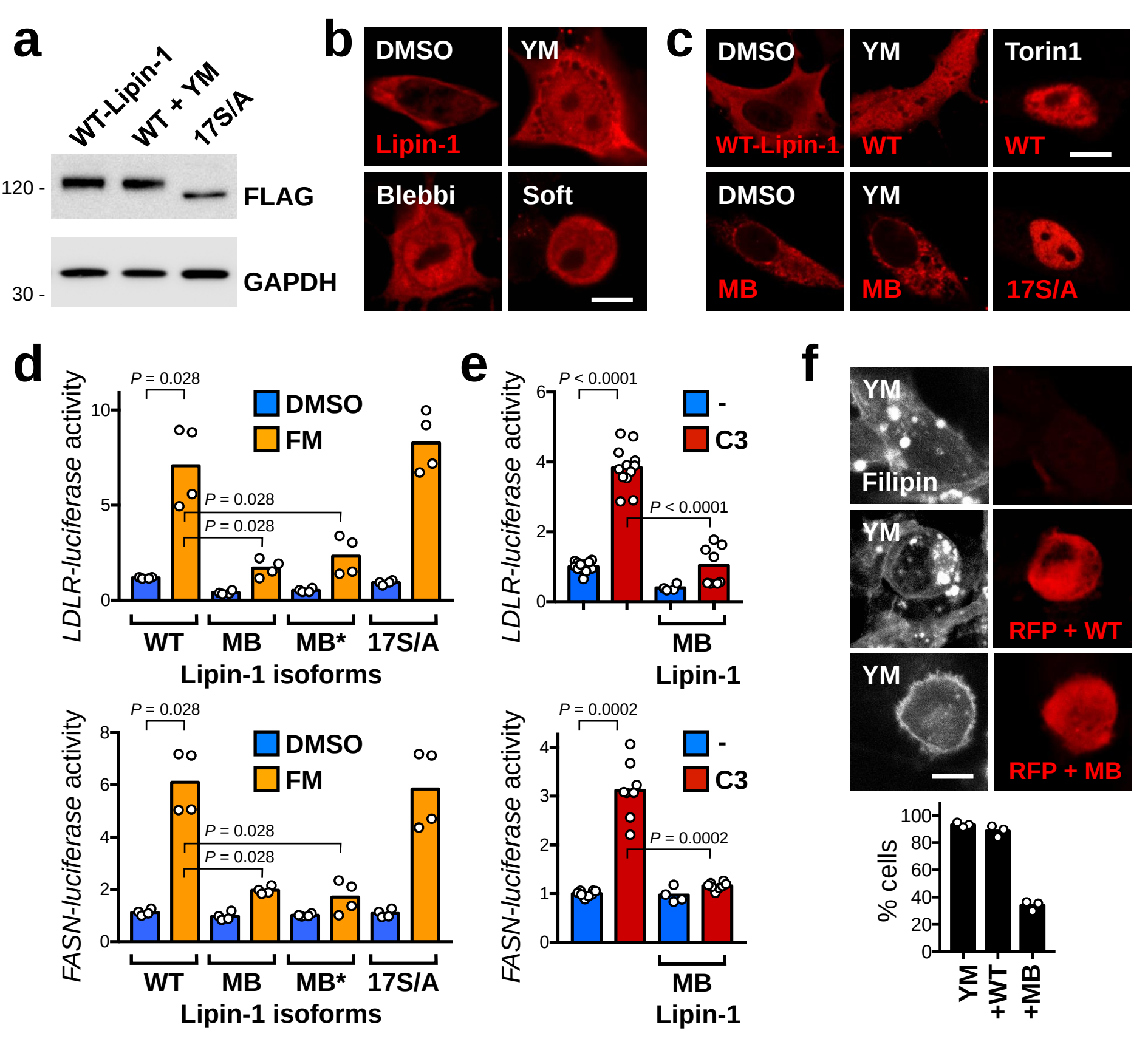
a
WT-Lipin-1
WT + YM
17S/A
120 -
FLAG
30 -
GAPDH
b
DMSO
YM
Lipin-1
Blebbi
Soft
c
DMSO
YM
Torin1
WT-Lipin-1
WT
WT
DMSO
YM
MB
MB
17S/A
d
LDLR-luciferase activity
P = 0.028
DMSO
FM
P = 0.028
P = 0.028
WT
MB
MB*
17S/A
Lipin-1 isoforms
FASN-luciferase activity
P = 0.028
DMSO
FM
P = 0.028
P = 0.028
WT
MB
MB*
17S/A
Lipin-1 isoforms
e
LDLR-luciferase activity
P < 0.0001
-
C3
P < 0.0001
MB
Lipin-1
FASN-luciferase activity
P = 0.0002
-
C3
P = 0.0002
MB
Lipin-1
f
YM
Filipin
YM
RFP + WT
YM
RFP + MB
% cells
YM
+WT
+MB

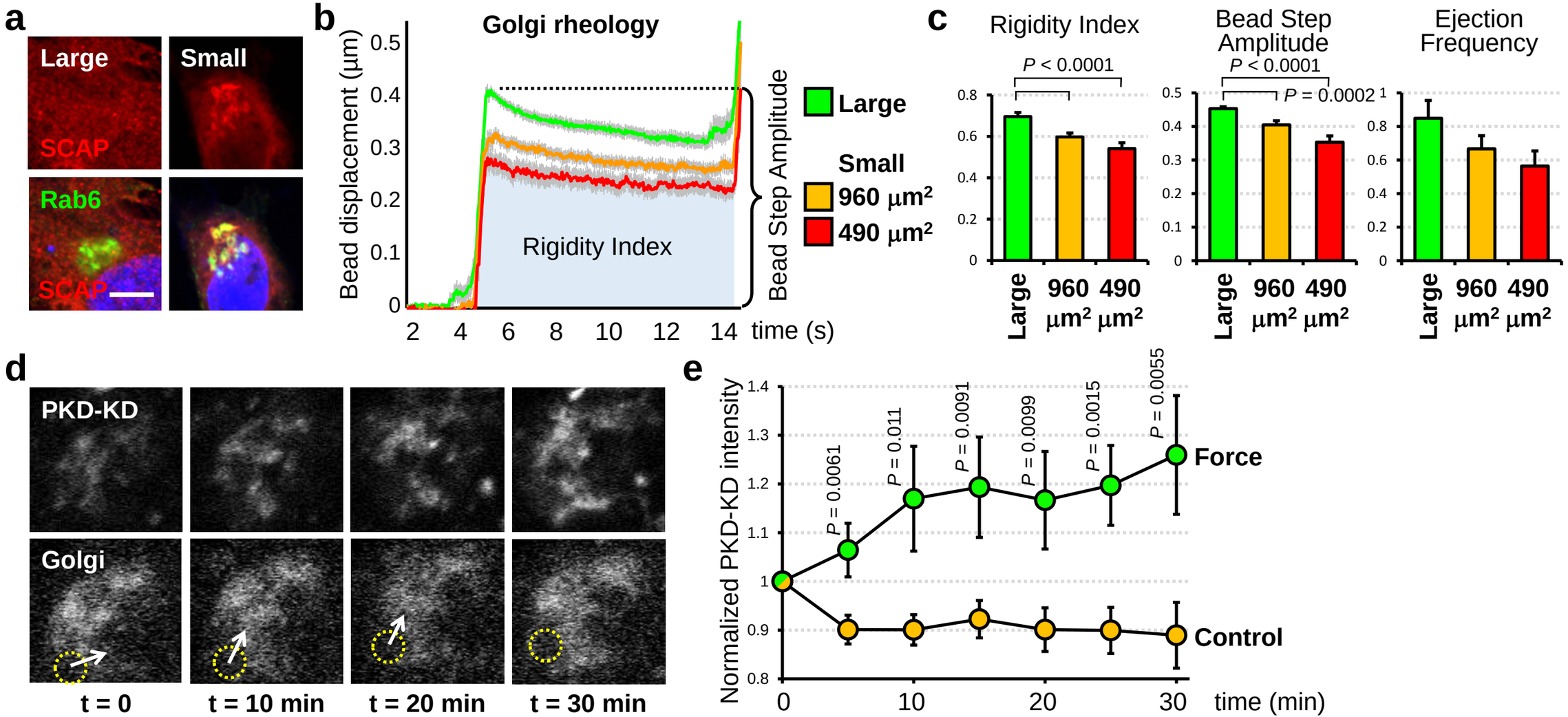
a
Large
Small
SCAP
Rab6
SCAP
b
Golgi rheology
Bead displacement (μm)
0.5
0.4
0.3
0.2
0.1
0
Rigidity Index
Bead Step Amplitude
Large
Small
960 μm²
490 μm²
2
4
6
8
10
12
14
time (s)
c
Rigidity Index
P < 0.0001
Bead Step Amplitude
P < 0.0001
P = 0.0002
Ejection Frequency
0.8
0.6
0.4
0.2
0
0.5
0.4
0.3
0.2
0.1
0
1
0.8
0.6
0.4
0.2
0
Large
960 μm²
490 μm²
d
PKD-KD
Golgi
t = 0
t = 10 min
t = 20 min
t = 30 min
e
Normalized PKD-KD intensity
1.4
1.3
1.2
1.1
1
0.9
0.8
P = 0.0061
P = 0.011
P = 0.0091
P = 0.0099
P = 0.0015
P = 0.0055
Force
Control
0
10
20
30
time (min)